Article

Developmental Cell

Synaptotagmin 4 Regulates Pancreatic β Cell Maturation by Modulating the Ca^{2+} Sensitivity of Insulin Secretion Vesicles

Graphical Abstract

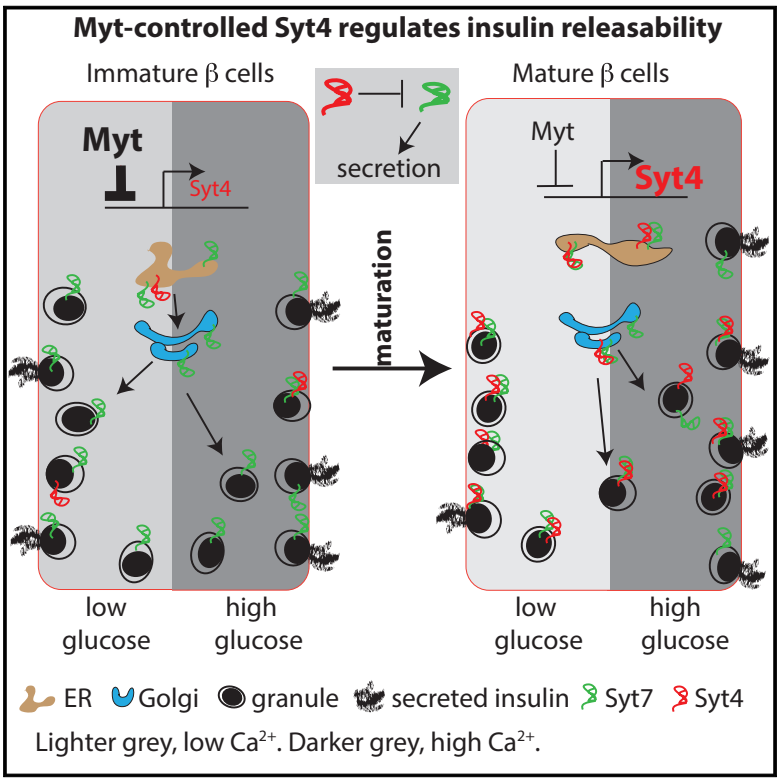

Highlights

- Immature β cells are more sensitive to Ca^{2+} stimulation during GSIS
- Increased Syt4 production promotes β cell maturation by reducing Ca^{2+} sensitivity
- Myt transcription factors repress the expression of *Syt4* in β cells
- Syt4, interacting with Syt7, regulates GSIS in mouse and human β cells

Authors

Chen Huang, Emily M. Walker, Prasanna K. Dadi, ..., Roland Stein, David A. Jacobson, Guoqiang Gu

Correspondence

david.a.jacobson@vanderbilt.edu (D.A.J.), guoqiang.gu@vanderbilt.edu (G.G.)

In Brief

In immature pancreatic beta cells, high glucose does not prompt an increase in insulin secretion. Huang et al. show that this poor response is due to greater Ca^{2+} sensitivity in immature cells, producing a higher basal secretion rate. Furthermore, Ca^{2+} sensitivity is regulated by synaptotagmin 4, whose levels increase during maturation.

Huang et al., 2018, Developmental Cell *45*, 347–361
May 7, 2018
https://doi.org/10.1016/j.devcel.2018.03.013

CellPress

Developmental Cell
Article

Synaptotagmin 4 Regulates Pancreatic β Cell Maturation by Modulating the Ca^{2+} Sensitivity of Insulin Secretion Vesicles

Chen Huang,[1,2,3] Emily M. Walker,[4] Prasanna K. Dadi,[4] Ruiying Hu,[1,2,3] Yanwen Xu,[1,2,3] Wenjian Zhang,[5] Tiziana Sanavia,[6] Jisoo Mun,[1] Jennifer Liu,[7] Gopika G. Nair,[7] Hwee Yim Angeline Tan,[8] Sui Wang,[9] Mark A. Magnuson,[1,2,4] Christian J. Stoeckert, Jr.,[10] Matthias Hebrok,[7] Maureen Gannon,[1,2,3,4,11] Weiping Han,[8] Roland Stein,[4] David A. Jacobson,[4,*] and Guoqiang Gu[1,2,3,12,*]

[1]Department of Cell and Developmental Biology, Vanderbilt University School of Medicine, Department of Veterans Affairs, Tennessee Valley Health Authority, Nashville, TN 37232, USA
[2]Center for Stem Cell Biology, Vanderbilt University School of Medicine, Department of Veterans Affairs, Tennessee Valley Health Authority, Nashville, TN 37232, USA
[3]The Program of Developmental Biology, Vanderbilt University School of Medicine, Department of Veterans Affairs, Tennessee Valley Health Authority, Nashville, TN 37232, USA
[4]Department of Molecular Physiology and Biophysics, Vanderbilt University School of Medicine, Department of Veterans Affairs, Tennessee Valley Health Authority, Nashville, TN 37232, USA
[5]China-Japan Friendship Hospital, Beijing 100029, P. R. China
[6]Department of Biomedical Informatics, Harvard Medical School, Boston, MA 02115, USA
[7]Diabetes Center, UCSF, San Francisco, CA 94143, USA
[8]Laboratory of Metabolic Medicine, Singapore Bioimaging Consortium, Singapore, Singapore
[9]Department of Ophthalmology, Mary M. and Sash A. Spencer Center for Vision Research, Stanford University School of Medicine, Palo Alto, CA 94304, USA
[10]Institute for Biomedical Informatics and Department of Genetics, University of Pennsylvania School of Medicine, Philadelphia, PA 19104, USA
[11]Department of Medicine, Vanderbilt University School of Medicine, Department of Veterans Affairs, Tennessee Valley Health Authority, Nashville, TN 37232, USA
[12]Lead Contact
*Correspondence: david.a.jacobson@vanderbilt.edu (D.A.J.), guoqiang.gu@vanderbilt.edu (G.G.)
https://doi.org/10.1016/j.devcel.2018.03.013

SUMMARY

Islet β cells from newborn mammals exhibit high basal insulin secretion and poor glucose-stimulated insulin secretion (GSIS). Here we show that β cells of newborns secrete more insulin than adults in response to similar intracellular Ca^{2+} concentrations, suggesting differences in the Ca^{2+} sensitivity of insulin secretion. Synaptotagmin 4 (Syt4), a non-Ca^{2+} binding paralog of the β cell Ca^{2+} sensor Syt7, increased by ~8-fold during β cell maturation. *Syt4* ablation increased basal insulin secretion and compromised GSIS. Precocious *Syt4* expression repressed basal insulin secretion but also impaired islet morphogenesis and GSIS. Syt4 was localized on insulin granules and Syt4 levels inversely related to the number of readily releasable vesicles. Thus, transcriptional regulation of *Syt4* affects insulin secretion; *Syt4* expression is regulated in part by Myt transcription factors, which repress *Syt4* transcription. Finally, human SYT4 regulated GSIS in EndoC-βH1 cells, a human β cell line. These findings reveal the role that altered Ca^{2+} sensing plays in regulating β cell maturation.

INTRODUCTION

Whole-body euglycemia is mediated in large part by insulin secreted from islet β cells. However, the precise mechanisms that govern insulin secretion, particularly in neonates, have not been completely characterized. In contrast to adult islet β cells, fetal and neonatal cells secrete more insulin in response to low basal glucose levels and have only modest glucose-stimulated insulin secretion (GSIS) (Grasso et al., 1968; Pildes et al., 1969). There are many potential stages at which GSIS can be regulated in β cells, including gap junctional or paracrine communication among islet cells, intracellular glucose metabolism, glucose-stimulated Ca^{2+} entry, as well as insulin vesicle formation, fusion, and release (Liu and Hebrok, 2017 and references therein). Understanding the post-natal maturation of the β cell secretory response will provide important insight for producing functional and therapeutically relevant β cells from human embryonic stem cells (ESCs)/induced pluripotent stem cells *in vitro*, as this process represents a major limiting step in their generation (Kieffer, 2016). Such knowledge will presumably also provide an understanding of islet β cell dysfunction in diabetes.

Several pathways and transcription factors (TFs) have been suggested to direct post-natal β cell development. For example, Ca^{2+}/calcineurin signaling facilitates β cell maturation by promoting insulin vesicle biogenesis (Goodyer et al., 2012); thyroid

hormones activate expression of the MafA TF (Aguayo-Mazzucato et al., 2013), which enhances the transcription of insulin and GSIS-related genes (Hang and Stein, 2011); secretory molecules, including Ucn3 from β cells (via somatostatin in δ cells [Blum et al., 2012; van der Meulen et al., 2015]) and neurotransmitters/hormones, can modulate β cell secretion by regulating β cell signal transduction or vesicular properties (Scarlett and Schwartz, 2015). Inactivation of several other TFs, including NeuroD (Gu et al., 2010) and Myt1 (Wang et al., 2007) reduce GSIS, suggesting that their roles in post-natal β cell maturation. In part, NeuroD1 functions through repression of glycolytic enzyme expression (Gu et al., 2010), although how Myt1 regulates β cell function remains unclear, largely due to the redundancy with two paralogs, *Myt1L* (*Nzf1*) and *St18* (*Nzf3*) (Wang et al., 2007). How these pathways and signals integrate to control the changes in β cell GSIS that occur during maturation remains unknown.

Changes in glucose metabolism and ATP-regulated channel activity play an important part in improving GSIS during β cell maturation (Rorsman et al., 1989). This entails reduced expression of various enzymes favoring glycolysis (e.g., hexokinases and lactate dehydrogenase, or disallowed factors) and increasing transcript abundance of those facilitating mitochondrial oxidative phosphorylation (Lemaire et al., 2016). The molecular mechanisms regulating the expression of these metabolic enzymes involve epigenetic modifications (Dhawan et al., 2015), microRNAs (Jacovetti et al., 2015), and nuclear receptors (Yoshihara et al., 2016).

Although changes in metabolism lead to changes in ion channel activity, these pathways are not sufficient to induce the alterations in GSIS that occur during β cell maturation. Notably, influx of Ca^{2+}, a key mediator of insulin secretion, is similar in P2 (2 days after birth) and adult β cells (Rozzo et al., 2009) even though physiological GSIS is not observed until post-natal day 9 (P9) or later (Blum et al., 2012; Nishimura et al., 2006). The number of releasable insulin vesicles does not limit the P2 GSIS response, since these β cells possess high basal and KCl-stimulated insulin secretion properties (Blum et al., 2012). These observations suggest that under-developed Ca^{2+}-secretion coupling of immature β cells could contribute to their impaired glucose responses. To this end, the availability of vesicles for release and/or Ca^{2+} sensitivity of vesicle fusion with the plasma membrane could contribute to this immaturity (Kalwat and Cobb, 2017). Indeed, many components of the SNARE (soluble N-ethylmaleimide-sensitive factor attachment protein receptor) vesicle fusion complex are Ca^{2+} sensitive, including syntaxin 1A, synaptosomal-associated protein 25, and synaptotagmins (Syts). The Syts are particularly interesting because they are known to regulate Ca^{2+}-secretion coupling in nerve cells (Craxton, 2004; Südhof, 2012). Although Syt7 is reported to promote insulin secretion (Dolai et al., 2016; Gustavsson et al., 2008; Wu et al., 2015), the broader influence of the Syt family of proteins in β cell maturation and GSIS is unknown.

There are 17 distinct Syt-encoding genes in mammals. Their ability to stimulate secretion depends on Ca^{2+} binding (Berton et al., 2000; Dean et al., 2009; Fukuda et al., 2003). Those that have a high affinity for Ca^{2+} (Syt1, 2, 3, 5, 6, 7, 9, and 10) can potentiate microsome fusion (Bhalla et al., 2008), while those which lack significant Ca^{2+} affinity repress SNARE-mediated membrane fusion (Bhalla et al., 2008; Littleton et al., 1999; Thomas et al., 1999). For example, Syt4 can inhibit vesicle secretion in cochlear inner ear hair cell synapses or PC12 cells (Johnson et al., 2010; Machado et al., 2004; Moore-Dotson et al., 2010), which involves direct binding of Syt4 to Ca^{2+}-sensitive Syt1 (Littleton et al., 1999).

Here we demonstrate that insulin vesicles in immature β cells have higher sensitivity to cytoplasmic Ca^{2+} levels, which is regulated by Syt4. Moreover, we provide evidence that elevated *Syt4* expression, partially regulated by Myt TFs, during β cell maturation plays a key role in regulating the GSIS response.

RESULTS

The Improvement in GSIS Is Not Regulated by Ca^{2+} Entry into Maturing Islet β Cells

Depolarization-induced Ca^{2+} entry is the trigger for insulin secretion in β cells (Rorsman and Renström, 2003). To examine if there was a difference in depolarization-stimulated insulin secretion (DSIS) between immature (P1 or P4) and mature islet β cells (P12 or adults), extracellular potassium was elevated to depolarize the cell membrane potential and activate voltage-gated Ca^{2+} channels (VGCCs). Glucose-independent DSIS occurred in each of these β cell populations (Figure 1A, left columns). Immature β cells actually showed greater (~4-fold) DSIS following a 10- or 45-min KCl stimulation (Figure 1A), a temporal response similar to the first and second phase of GSIS (Rorsman and Renström, 2003). Addition of 2.8 mM glucose during DSIS produced findings comparable with KCl alone, with immature β cells secreting ~4-fold more insulin than mature β cells (Figure 1A, right columns). The higher levels of insulin secretion in immature β cells could not be explained by the amount of insulin within each β cell, because mature cells contain 1.6-fold more insulin than immature β cells (Figure 1B). Nor is it a result of differing quantities of insulin in each vesicle, as the diameter of the dense insulin protein core was similar between immature and mature β cells (Figures S1A–S1E).

These findings suggest that immature β cells undergo a greater number of secretion events following a depolarizing stimulus than mature cells, which might be explained by differences in cytoplasmic Ca^{2+} handling. Although KCl treatment induced β cell cytoplasmic Ca^{2+} influx in islets of all stages (Figure 1C), the total amount of KCl-induced Ca^{2+} entry was significantly higher in mature β cells compared with immature β cells (Figures 1D and 1E). However, immature β cells (P1, P4) had a higher concentration of basal cytoplasmic Ca^{2+} compared with mature β cells (P12, adult [Blum et al., 2012]) (Figure 1C, ~120%), consistent with their higher glycolysis rate (Jermendy et al., 2011). These data suggest that the greater DSIS in immature β cells is not a result of elevated Ca^{2+} influx.

It is also possible that changes in VGCC isoforms or subcellular localization influence Ca^{2+} entry and insulin secretion during maturation. To test this, we monitored insulin secretion from islets treated with a K^+ channel activator (i.e., diazoxide) and an ionophore (ionomycin) to induce equivalent Ca^{2+} entry across the entire β cell membrane without VGCC activation (Do et al., 2014). Under these conditions, the immature islets again showed ~3-fold higher insulin secretion compared with

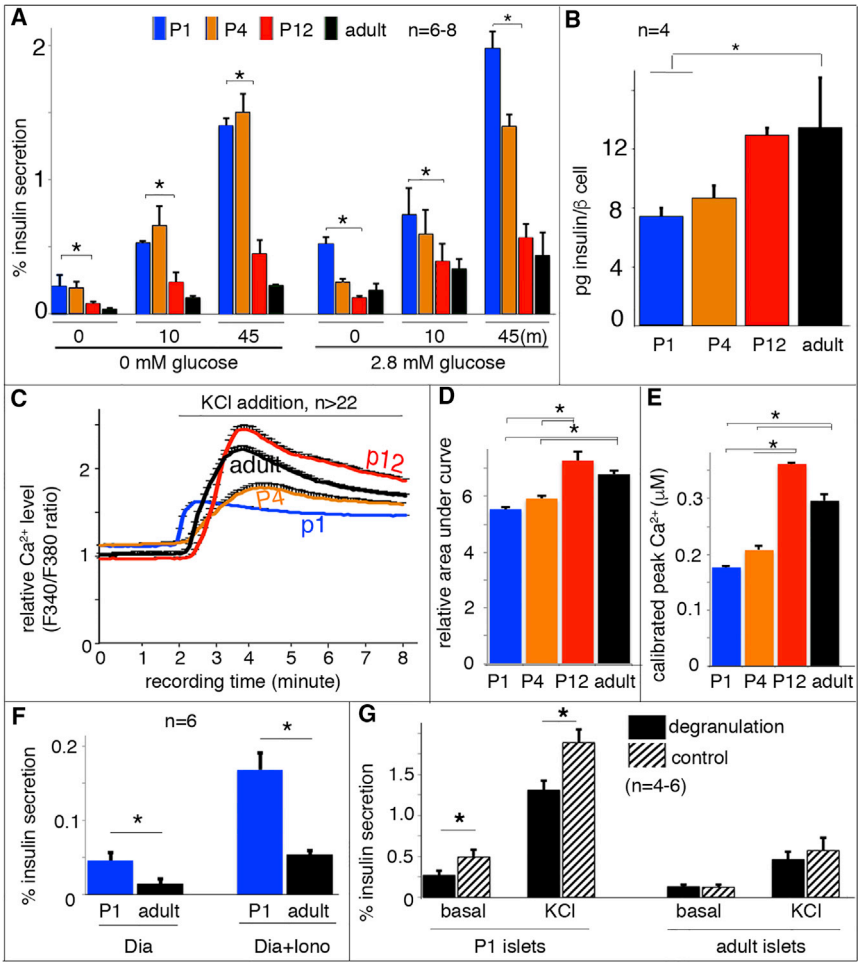

Figure 1. Equivalent Ca^{2+} Influx Results in More Insulin Secretion in Immature β Cells

Handpicked islets were used for secretion and Ca^{2+} assays.

(A) The percentage of insulin secretion induced by 25 mM KCl in islets at 0 (left columns) or 2.8 mM (right columns) glucose. Data from three time points, before KCl stimulation ("0"), 10 or 45 min (m) with KCl stimulation ("10" or "45") were presented. The data at 0 min represent insulin secretion within a 45-min time window without KCl stimulation. The indicated statistical analysis (top brackets) was calculated between P1 and P12 islets.

(B) Insulin content per β cell, assayed with purified β cells of *Rip*^{mCherry} mice.

(C) Average islet cytoplasmic Ca^{2+} responses to 25 mM KCl-induced depolarization in 2.8 mM basal glucose; these responses were assayed with Fura2AM.

(D) Quantification of the KCl-induced islet Ca^{2+} response defined with area-under-curve after KCl addition (from 2 to 8 min).

(E) The greatest total Ca^{2+} levels reached in islets of different ages stimulated by 25 mM KCl.

(F) Insulin secretion induced by ionomycin (Iono) in P1 and adult islets. Diazoxide (Dia) was included in these assays.

(G) Islet DSIS with or without glucose-induced degranulation, achieved by incubating islets in 5.6 mM glucose for 1 hr prior to DSIS.

Error bars represent the SEM. *p < 0.05, t test.

mature islets (Figure 1F), suggesting that the hyper insulin secretion in immature β cells does not depend on particular sites of Ca^{2+} entry.

Since immature β cells secrete a greater percentage of total cellular insulin content, it was predicted that prolonged stimulation would deplete the readily releasable insulin vesicle. This was tested by pre-incubating islets with 5.6 mM glucose for 1 hr (degranulation), which will only stimulate high insulin secretion from the immature β cells. As expected, there was significant reduction of DSIS in immature β cells following pre-incubation in 5.6 mM glucose (degranulation) compared with untreated controls, but no reduction in adult islets (Figure 1G).

Increasing cAMP levels stimulate GSIS in a Ca^{2+}-independent fashion (Ammälä et al., 1993). Yet, elevating the intracellular cAMP level with 3-isobutyl-1-methylxanthine, an inhibitor of the phosphodiesterase that degrades cAMP, potentiated DSIS by ~5-fold in adult islets and only ~2-fold in P1 (Figure S1F). This finding suggests that the cAMP-mediated pathway is less active in immature β cells and unlikely to account for their hypersensitive Ca^{2+}-secretion coupling.

Collectively, our results imply that the greater DSIS of immature β cells is not a result of elevated depolarization-induced Ca^{2+} influx or cAMP generation. Hence, we found that the insulin vesicles in immature β cells undergo greater Ca^{2+}-induced fusion with the plasma membrane than adult islet cells, conditions producing less cAMP. In the following experiments, we will show that Syt4 regulates vesicle sensitivity to Ca^{2+} and GSIS during β cell maturation.

Increased Syt4 Expression Correlates with β Cell Maturation

RNA sequencing (RNA-seq) was performed on β cells purified from P1, P12, and P60 *Mip*^{eGFP} mouse islets to identify gene networks that change over the β cell maturation process. P1 represented immature β cells, P12 represented β cells that have proper GSIS with no exposure to the post-weaning high carbohydrate diet (Blum et al., 2012), and P60 represented adult functional β cells (Stolovich-Rain et al., 2015). As expected, most of the genes known to promote β cell maturation, including *MafA*, *NeuroD1*, and *Ucn3* (Table S1), displayed significantly increased expression from immature to mature state.

We focused here on vesicular genes that could regulate Ca^{2+}-secretion coupling. Eight of the 17 *Synaptotagmin* genes (*Syt*) were expressed in these β cell populations (i.e., *Syt3, 4, 5, 7, 9, 11, 13,* and *14*; Table S1). The expression change in each of these key SNARE gene products was verified by real-time RT-PCR in FACS-purified P1, P12, and adult β cells from a second mouse line, *Rip*^{mCherry} mice. No significant difference was found

in *Syt5*, *Syt7*, *Syt9*, and *Syt13* levels, whereas the mRNA levels of *Syt3*, *Syt4*, *Syt11*, and *Syt14* increased during islet maturation (Figure S2A, repeated measure ANOVA, $p \leq 0.019$). Notably, only *Syt4* and *Syt14* displayed significant expression changes (~>5-fold) between the P1 and P12 islets (t test; $p \leq 0.04$). Subsequent analysis focused on *Syt4* because its transcript levels were ~8-fold higher than *Syt14* (Figure S2A). Most importantly, this resulted in increased Syt4 production during the process of β cell maturation (Figure 2A).

Syt4 Localizes to Both Vesicles and Non-vesicular β Cell Compartments

Super-resolution structured illumination microscopy (SIM) was used to determine the subcellular localization of Syt4 in β cells. SIM clearly resolved the structure of individual vesicles (Figure 2B1). Importantly, we observed that a majority of insulin vesicles co-localized with Syt4 signals (Figure 2B2), which also displayed granular non-uniform distribution (Figure 2B3). The co-localization of Syt4-insulin signals was seen under 3D projection (Figure 2B) as well as single optical slice images (Figure 2C). A small portion of bright insulin vesicles (~10% in 50 β cells examined with strong insulin immunofluorescence signals) did not co-localize with Syt4 (Figure 2B2, arrowheads). Why these vesicles are different from the rest of the pool is not clear, but they may have no or only low levels of Syt4, or they may be vesicles in the process of being degraded by autophagy. Interestingly, some strong Syt4 signals did not co-localize with insulin vesicles (Figures 2A–2C and S2B), but in the Golgi (Figures S2C and S2D) and the endoplasmic reticulum (ER) (Figures S2E and S2F). Although the role of Syt4 in ER and Golgi biology will be addressed elsewhere, we focused on the potential role of Syt4 in regulating Ca^{2+}-induced insulin secretion.

Syt4 Is Required for β Cell Maturation

Syt4 knockout ($Syt4^{-/-}$) mice were used to determine the functional involvement of this protein in islet β cells. Eight-week-old $Syt4^{-/-}$ mice displayed a modest, but significant, defect in glucose clearance (Figure 2D), despite their normal insulin sensitivity (Figure 2E). In addition, $Syt4^{-/-}$ serum insulin levels were lower during glucose tolerance tests (Figure 2F). GSIS in 8-week-old $Syt4^{-/-}$ islets was also blunted compared with controls (Figure 2G). At P10 and adult stages, $Syt4^{-/-}$ islet and vesicular morphology was unchanged, as were the levels of many key endocrine genes associated with cell activity, including the endocrine hormones, the *Glut2* glucose transporter, and key islet TFs (*MafA*, *MafB*, *Pdx1*, and *Nkx6.1*) (Figure S3 and data not shown). These observations indicated that the Syt4 effect on insulin secretion *in vivo* was not mediated by changes in islet cell identity or vesicular biosynthesis, but the response of vesicles to glucose stimulation.

Interestingly, a significantly higher basal GSIS was observed in pre-weaned, 2-week-old $Syt4^{-/-}$ islets (Figure 2H), implying that Syt4 increases the threshold of Ca^{2+} needed to trigger insulin secretion. However, the response of these islets to high glucose levels remained largely normal at this stage (Figure 2H), indicating an overall leftward shift of Ca^{2+} sensitivity. This possibility was examined using DSIS by pre-incubating mutant and control islets in Krebs-Ringer bicarbonate buffer without glucose for 1 hr in order to prevent glucose-induced degranulation. DSIS from non-degranulated $Syt4^{-/-}$ islets was significantly higher than control islets (Figure 2H), supporting the hypothesis that Syt4 reduces Ca^{2+}-sensitive insulin vesicle fusion with the plasma membrane. Notably, preventing degranulation before the DSIS normalized insulin secretion at basal conditions (physiological KCl) in control and $Syt4^{-/-}$ islets, because of the increased basal secretion in control cells (Figure 2H, showing the basal insulin secretion levels in control islets with GSIS versus DSIS). These changes in DSIS in $Syt4^{-/-}$ islets were not due to Ca^{2+} handling, since P14 control and $Syt4^{-/-}$ islets had similar Ca^{2+} influx properties during both glucose stimulation and KCl-induced depolarization (Figures 2I and 2J).

Syt4 Overexpression Represses Basal Insulin Secretion and Impairs Islet Morphogenesis

We next examined whether precocious Syt4 overexpression (Syt4OE) would expedite β cell maturation. Three *TetO*-inducible transgenic mouse lines (termed nos 1, 2, and 3) were derived that enabled inducible Syt4 production in $TetO^{Syt4}$; Rip^{rTTA} ($Syt4^{OE}$) β cells. $Syt4^{OE}$ embryos/mice were exposed to doxycycline (Dox) from embryonic day 16.5 (E16.5) via drinking water from the plugged mice (Figure 3A). This procedure induced detectable Syt4OE only after E17.5, which reached ~6-fold in P2 islets in all three lines (Figure 3B). Line numbers 1 and 2 were used to test the physiological effects of Syt4OE in β cells, which resulted in significantly repressed basal insulin secretion in perinatal islets at P4 and P7, but without significant effect on GSIS (Figure 3C). Corresponding to the reduced basal insulin secretion, 2-week-old $Syt4^{OE}$ mice displayed a trend of higher random blood glucose levels (i.e., ~20%; Figure 3D).

We examined the islet morphologies and gene expression patterns in P4 pancreatic sections of $Syt4^{OE}$ pancreas to determine if the observed differences in insulin secretion resulted from abnormal β cell development. No differences were observed in the expression levels/patterns of endocrine hormones (indicative of islet morphogenesis) and key β cell markers including *MafA*, *MafB*, *Pdx1*, and *Glut2* (Figures S4A and S4B). These findings, together with the P4 insulin secretion profiles, suggest that Syt4OE reduced basal insulin secretion without compromising β cell development or islet morphogenesis.

Interestingly, at P10, $Syt4^{OE}$ islets showed noticeable abnormalities in islet morphology, gene expression, and β cell proliferation. At this stage, >83% of islets had the typical β cell-enriched core organization (Figure 3E1). Only 51.4% ± 3.4% of $Syt4^{OE}$ islets had this architecture, with nearly half displaying non-β cells in the core of islets (Figure 3E2). Moreover, $Syt4^{OE}$ β cells had reduced Glut2 and increased MafB levels in β cells (Figures 3F and 3G). In contrast, expression of several other TFs was unaffected, including *MafA, Myt1, Nkx6.1,* and *Pdx1* (Figures S4C and S4D). Furthermore, islet β cell proliferation was significantly compromised at P10 as assayed with Ki67 positivity (Figures 3H and 3I), which resulted in reduced β cell mass (Figure 3J).

The abnormal islet phenotype of $Syt4^{OE}$ mice persisted for nearly 4 weeks after cessation of Syt4OE upon Dox withdrawal (P35), with non-β cells consistently observed in the center of islets (Figure 3K) and reduced Glut2 levels on the β cell membrane (Figure 3L). In contrast, *MafB* expression was reduced to undetectable levels in β cells (Figure 3M). GSIS was also compromised in $Syt4^{OE}$ islets (Figure 3N), and there was a trend

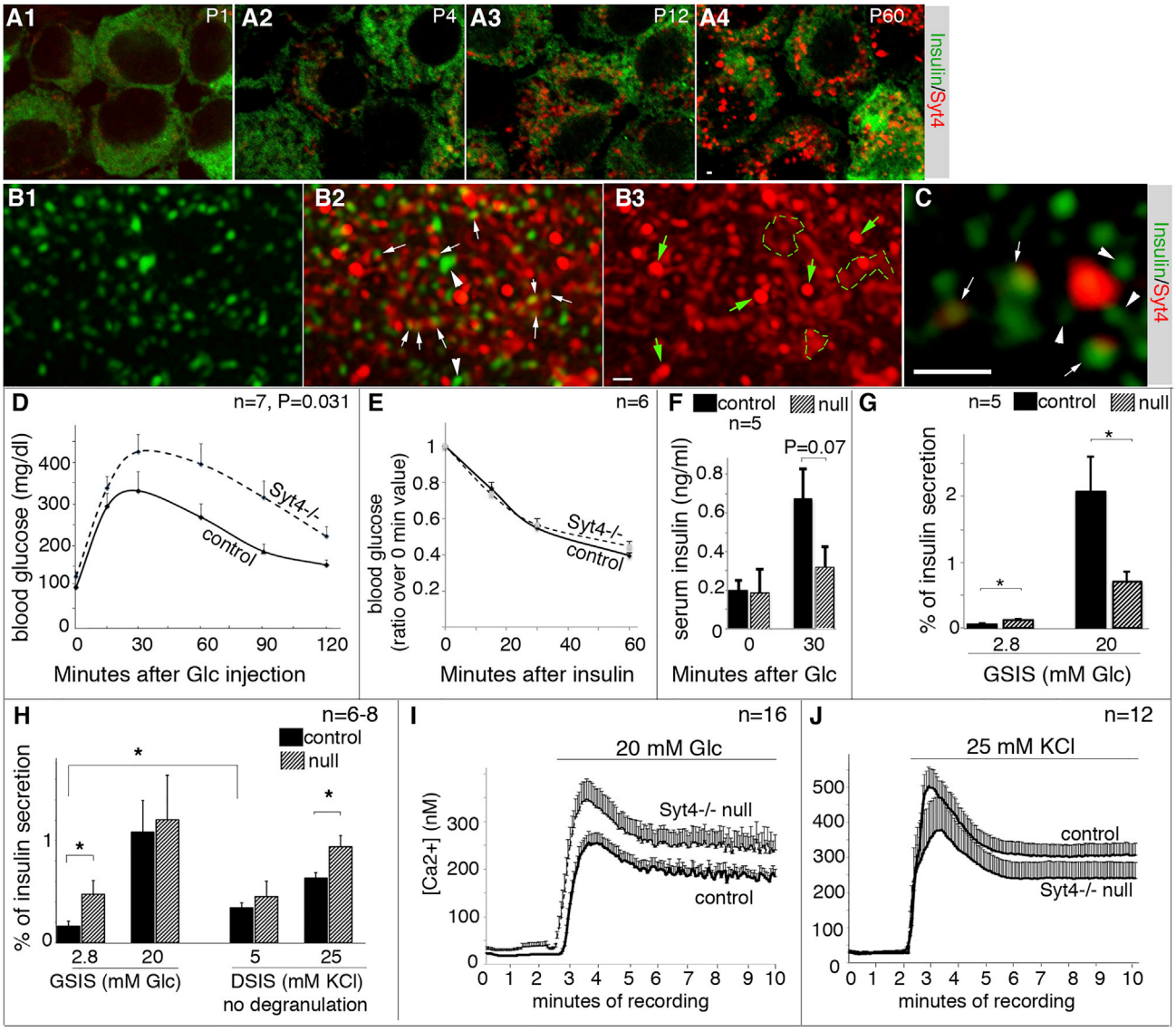

Figure 2. Increased *Syt4* Expression Is Required for β Cell Maturation

(A) Laser scanning microscopy (LSM) confocal images of Ins/Syt4 immunofluorescence in P1 to adult β cells. Single optical slices of merged images are shown, taken under identical confocal parameters. Note that isolated islets were partially dissociated and quickly attached onto slides with cytospin methods, followed by fixation and staining. Under this condition, the islet vesicles appeared disrupted so that insulin immunofluorescence appeared as diffusive signals. Scale bar, 1 μm.

(B) SIM images of Ins/Syt4 staining in a representative adult β cell. Shown are projections of 8 optical slices taken 125 nm apart, with insulin (B1), merged (B2), and Syt4 channel (B3) shown. Arrows and arrowheads in B2 show examples of vesicles with or without co-localizing Syt4 signals. Green arrows and broken circles in B3 highlight Syt4 patches devoid of Ins signals. Scale bar, 1 μm.

(C) An enlarged single optical slice (~100 nm thickness) to highlight the co-localization of Ins and Syt4 in several vesicles (arrows). Arrowheads point to several vesicles that are close but not contacting the Syt4 signals. Scale bar, 1 μm.

(D) IPGTT in 8-week-old control (wild-type) and *Syt4* null mice. The p value is calculated with repeated measures ANOVA. Glc, glucose.

(E) Insulin sensitivity assay in 8-week-old mice after 4 hr fasting. Presented are the ratios of blood glucose levels over that before insulin injection.

(F) Serum insulin levels detected during IPGTT test (8-week-old mice).

(G) GSIS of 8-week-old *Syt4*$^{-/-}$ islets.

(H) GSIS and DSIS of P14 islets.

(I and J) P14 islet cytoplasmic Ca^{2+} induced by 20 mM glucose (I) or 25 mM KCl (J).

Error bars represent the SEM. *p < 0.05, t test.

toward defective glucose clearance in post-weaning mice (Figure 3O, p = 0.06 with repeated measure ANOVA. p < 0.05 for time points 30 and 60 min, t test). These data suggest that transient *Syt4* overexpression at neonatal stages, through repressing basal secretion, has long-lasting detrimental effects on islet morphogenesis and function.

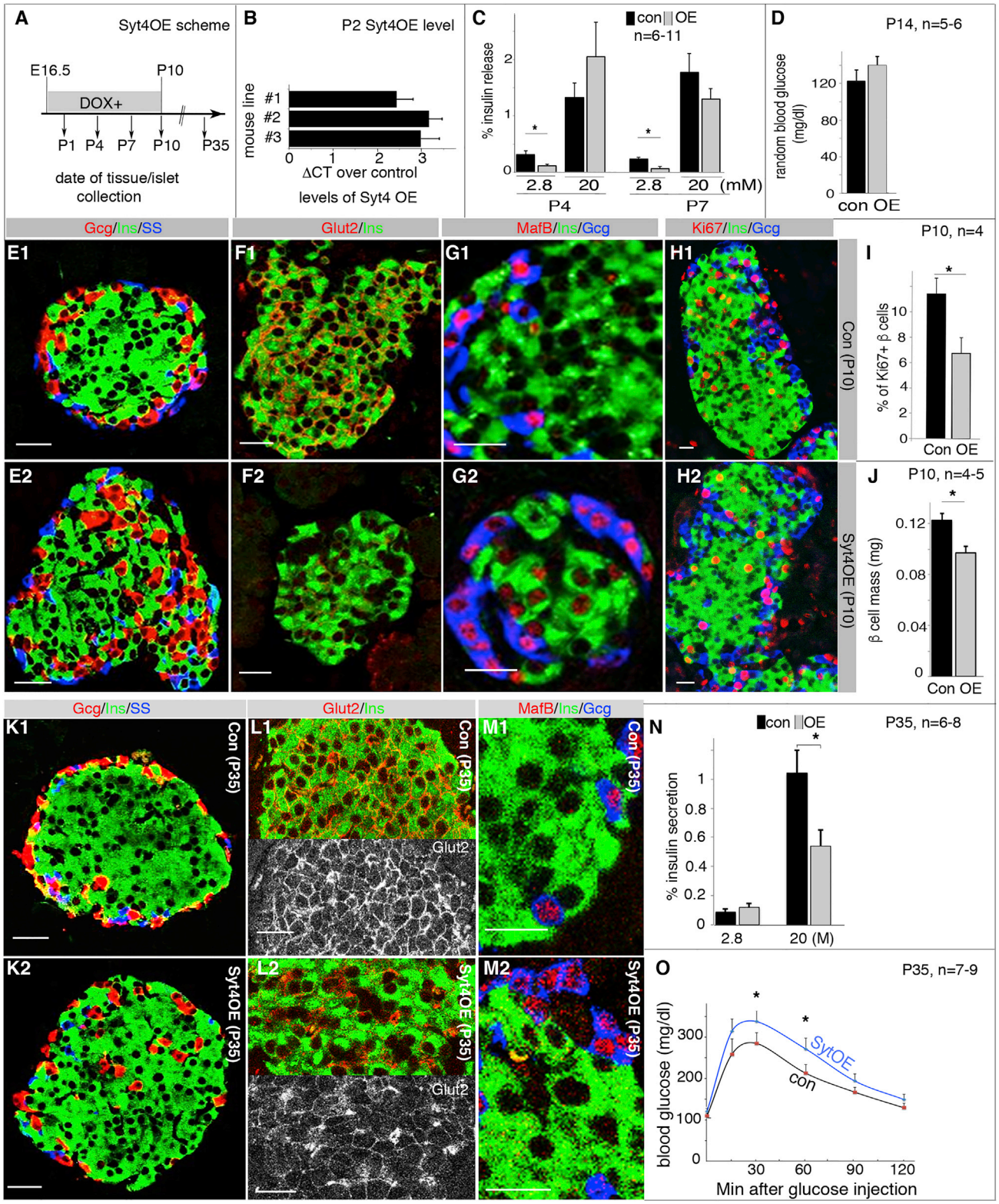

Figure 3. *Syt4*^{OE} Promotes β Cell Maturation but Impairs Islet Morphogenesis and GSIS

Control ([con], including *TetO*^{Syt4} and *Rip*^{rTTA} mice) and *Syt4*^{OE} littermates were used for all assays. Images were captured with identical parameters.

(A) The time frame used for Dox administration and islet/mouse characterization. After intercrossing, Dox feeding started at E16.5 in plugged females and last to P10, or to the point of tissue collection before P10.

(legend continued on next page)

Syt4 Partially Co-localizes and Interacts with Syt7 in Islet β Cells

We next explored if interactions between Syt4 and other family members could influence insulin secretion, a mechanism used to regulate Ca^{2+}-induced secretion in neurons. For example, Syt4 binding to Syt1 reduces the efficiency of vesicle plasma membrane fusion induced by Ca^{2+} (Bhalla et al., 2008; Littleton et al., 1999). Notably, the *Syt1* functional paralog, *Syt7*, is highly expressed in β cells and has been found to act as a Ca^{2+} sensor to promote insulin secretion (Dolai et al., 2016; Gustavsson et al., 2008; Wu et al., 2015).

Syt7 was detected in the majority of insulin vesicles and non-vesicular compartments when assayed using SIM, in both maxi-projection (Figure 4A) and single optical slice images (Figure 4B). Furthermore, Syt7 partially co-localized with Syt4 in dispersed islet β cells (Figure 4C). Proximity ligation analysis showed that Syt4 and Syt7 localized very close to each other (<40 nm, Figures 4D and 4E), suggesting their direct interaction. Indeed, interaction between these proteins was also observed in co-immunoprecipitation assays performed in 293 cells with Syt mutant fragments lacking their transmembrane domains to minimize non-specific binding (Figure 4F). Moreover, insulin secretion was severely attenuated in immature $Syt7^{-/-}$ islets (Figure 4G). These data are consistent with Syt4:Syt7 interactions reducing Ca^{2+}-induced insulin secretion in maturing β cells.

Syt4 Regulates Insulin Vesicle Localization to the Plasma Membrane

Syt7 has been found to promote insulin vesicle transport to the cell membrane (Dolai et al., 2016; Osterberg et al., 2015). Consequently, transmission electron microscopy (TEM) was used to determine if Syt4, presumably through interaction with Syt7, could also affect insulin vesicle density on/near the plasma membrane.

Although Syt4OE did not significantly change the size of mature insulin vesicles (recognized by their dense core surrounded by a ring of electron light materials, arrows in Figures 5A, 5B, and S5), it caused a ~20% increase in the number of mature vesicles in β cells at P4 and P7 (Figure 5E). In addition, Syt4OE reduced the number of insulin vesicles docked within 20 nm of the plasma membrane (Figure 5F). In contrast, neither insulin vesicle size nor density was changed in $Syt4^{-/-}$ β cells (Figure S5B), but docked vesicles density was increased in P14 β cells when the endogenous Syt4 levels were high (Figures 5C–5F). Interestingly, $Syt4^{-/-}$ β cells have a reduction in the number of docked vesicles just after weaning at P24, which is consistent with the reduced GSIS in post-weaning $Syt4^{-/-}$ islets (Figure 2G). These combined findings suggest that Syt4 regulates the localization of insulin vesicles to the cell membrane.

Myelin TFs (Myt) Regulate Syt4 Expression

We searched for the TFs that regulate the expression of *Syt4.* Inactivation of *MafA* did not change the expression of *Syt4* (Artner et al., 2010). Strikingly, we found that total loss of *Myt1, Myt1L,* and *St18* production in pancreatic progenitors yielded a phenotype similar to $Syt4^{OE}$ islets. Our previous work demonstrated that expression of the *Myt1* paralogs, *Myt1L* and *St18*, were induced in the embryonic $Myt1^{-/-}$ pancreas, a mutant mouse with deficiencies in GSIS in adult islets (Wang et al., 2007). Furthermore, we found that all three factors were produced in post-natal islet cells (Figure 6A). To address the overall significance of the Myt family in the pancreas, all three *Myt* genes were inactivated in pancreatic progenitors using $Pdx1^{Cre}$ and newly derived $Myt1L^{F}$ and $St18^{F}$ floxed alleles (Figure S6). This allowed for efficient inactivation of all three genes in the endocrine islets of $Myt1^{F/F}$; $Myt1L^{F/F}$; $St18^{F/F}$; $Pdx1^{Cre}$ mice (termed *6F; Cre,* Figure 6B).

The body weight and blood glucose levels of neonatal *6F; Cre* mice were normal until about 1 week after birth compared with wild-type, $Myt1^{F/F}$; $Myt1L^{F/F}$; $St18^{F/F}$ *(6F),* and $Pdx1^{Cre}$ control mice. Yet the *6F; Cre* mice developed elevated fasting blood glucose several days after weaning (Figure 6C), concomitant with reduced GSIS and DSIS, like $Syt4^{OE}$ islets (compare Figure 6D with Figure 3N). The *6F; Cre* islets lacked visible defects in their insulin levels, assayed by insulin immunofluorescence (Figure 6E), and vesicular morphology, determined with TEM (Figure 6F). These results suggest the involvement of Myt factors with β cell function, likely involved the maturation steps.

RNA-seq was performed to analyze *Syt4* levels in purified β cells by virtue of Mip^{eGFP} expression from newly born (P1) *6F; Cre;* Mip^{eGFP} and control Mip^{eGFP} islets. There was a significant 2.4-fold upregulation of *Syt4* in *6F; Cre* β cells (Figure 6G). Interestingly, we also observed significant upregulation of *NeuroD1* (1.6-fold, $p = 0.002$) and trends of upregulation of *Ucn3* ($p = 0.14$) and *MafA* ($p = 0.16$). The expression of *Nkx6.1* and *Pdx1* was unchanged, and *Glut2* expression was significantly decreased in the *6F; Cre* β cells (Figure 6G). Increased *Syt4* expression was also observed in P14 islets (Figure 6H), although the expression of the other genes except *Glut2* was normalized (data not shown).

The above findings suggest that the loss of Myt factors have de-repressed *Syt4* transcription, and that a normal function of Myt proteins is to repress *Syt4*. This conclusion predicts that *Myt* expression levels could decrease during β cell maturation to allow for *Syt4* upregulation. Indeed, the *Myt1* expression level showed a significant reduction from P1 immature to P12/adult mature β cells, at both mRNA (Figure 6I) and protein levels (Figures 6J–6M), whereas the expression levels of *Myt1L* and *St18* stayed relatively unchanged (Figure 6I).

(B) Real-time RT-PCR showing *Syt4* overexpression in isolated P2 islets of three independent mouse lines.
(C) GSIS in P4 and P7 $Syt4^{OE}$ islets. Shown are the percentages of insulin secretion within a 45-min time window.
(D) Random feeding blood glucose in control (con) and $Syt4^{OE}$ (OE) mice.
(E–G) Immunoassays in P10 islets with/without $Syt4^{OE}$, highlighting islet morphology (E), Glut2 (F), and MafB production (G).
(H and I) β cell proliferation assays and quantification with Ki67 labeling in P10 islets.
(J) β Cell mass in P10 pancreata.
(K–M) Gene expression in P35 islets in mice with/without transient $Syt4^{OE}$ between E16.5 and P10. Panels L1 and L2 were split, with a single Glut2 channel to highlight the change in Glut2 levels.
(N and O) Islet GSIS and IPGTT assays in P35 control and $Syt4^{OE}$ mice.
Error bars represent the SEM. Scale bars, 20 μm. *$p < 0.05$, t tests.

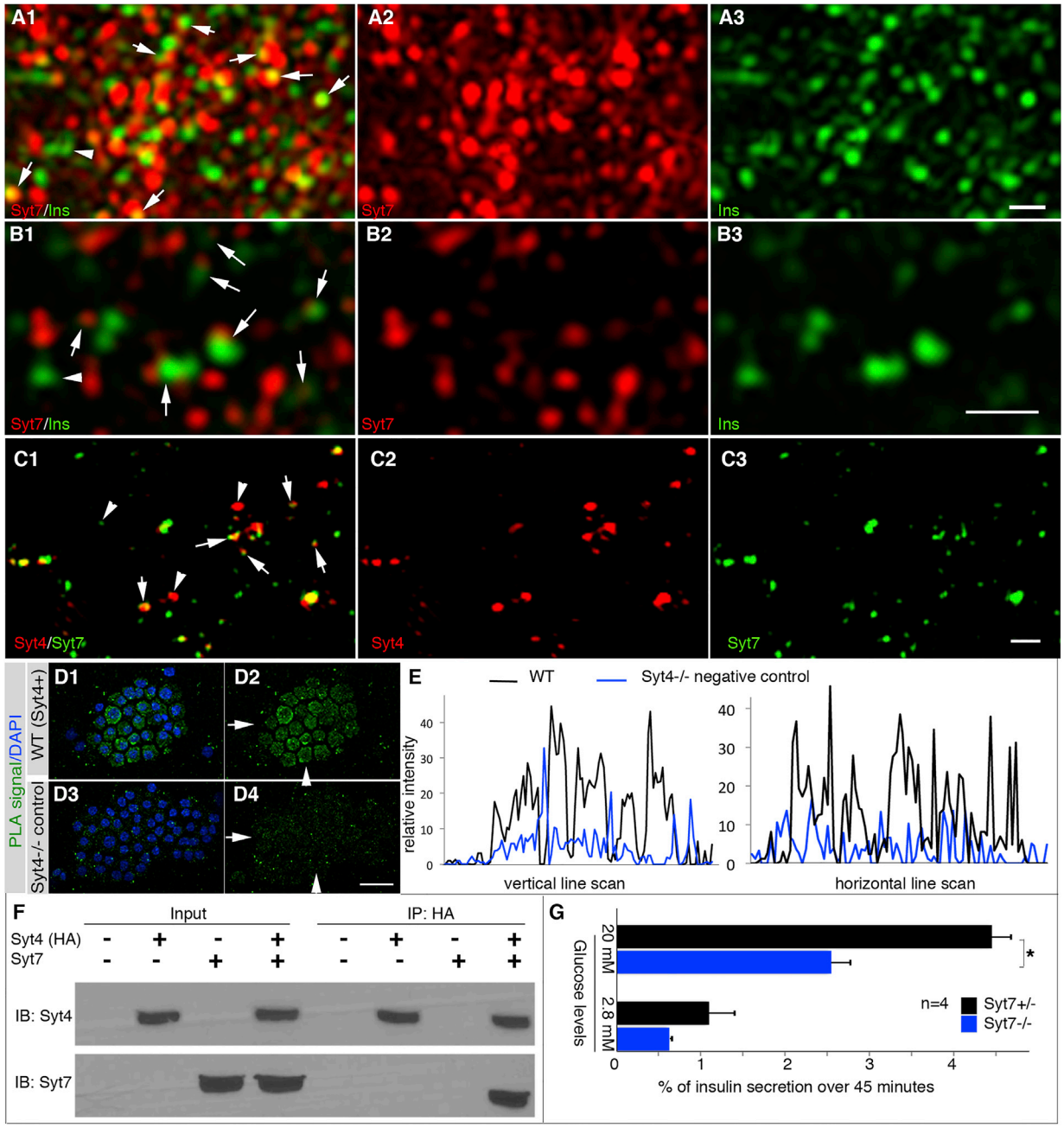

Figure 4. Syt4 Co-localizes with Syt7 in β Cells

(A and B) SIM images showing the subcellular localization of Syt7 in a representative adult β cell. Panels in (A) are projections of 8 optical slices taken 125 nm apart. Panels in (B) are single SIM slices for better resolution of Ins/Syt7 localization. Note the large portions of vesicles with overlapping/close localization of Ins/Syt7 (arrows in A1 and B1). Also note the vesicles without obvious contact with Syt7 (arrowheads).

(C) Co-localization of Syt4 and Syt7 in β cells shown with SIM. Arrows, spots of Syt4-Syt7 co-localization. Arrowheads, spots of single Syt4 or Syt7 signal. The cell identity is confirmed by insulin expression, not included here. Scale bars, 0.5 μm.

(D and E) Proximity ligation analysis (PLA) assays verifying the close localization of Syt4 and Syt7, accepted as indication of direct association. Hand-picked islets attached onto slides with the cytospin method were used. Images were captured with LSM, and z stack images are presented to show signals in the entire cell (D). Note that merged images (D1 and D3) between DAPI and PLA signal and single PLA signal images (D2 and D4) are shown. *Syt4*$^{-/-}$ islet cells (D3 and D4) are included as negative controls. Arrows and arrowheads in D2 and D4 are the positions of line-scan to compare the relative PLA signal intensity presented in (E), in horizontal and vertical directions. Scale bar, 20 μm.

(F) Immunoprecipitation showing Syt4-Syt7 interactions. Lysates from HEK293 cells transfected with constructs that expressing hemagglutinin (HA)-tagged Syt4 and Syt7 cytoplasmic domains were used. Proteins were immunoprecipitated by anti-HA, then immuno-blotted with anti-Syt7 antibodies.

(G) GSIS of P4 *Syt7*$^{-/-}$ and control immature islets. *p = 0.02, t tests.

Error bars represent the SEM.

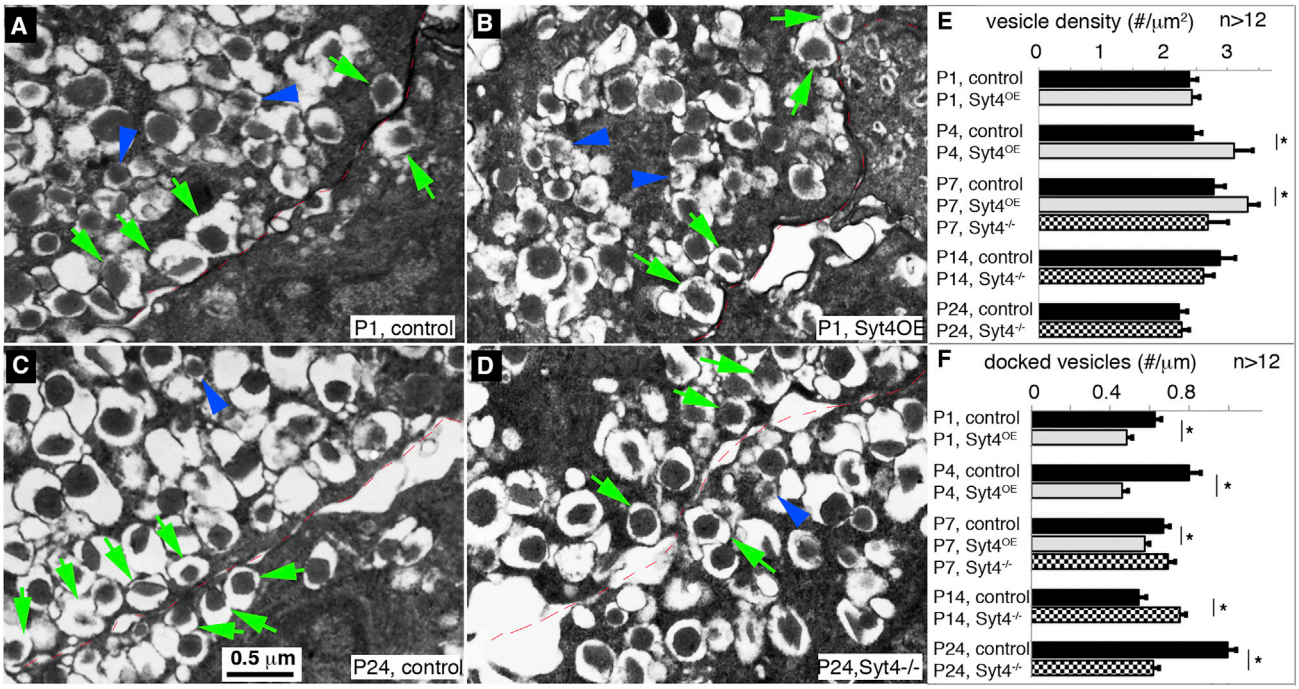

Figure 5. Syt4 Regulates Insulin Vesicle Docking to the Plasma Membrane

(A–D) Representative TEM images of β cells with *Syt4* overexpression or inactivation. (A and B) P1 control and $Syt4^{OE}$ β cells. (C and D) P24 control and $Syt4^{-/-}$ β cells. Green arrows point to several examples of docked mature vesicles. Blue arrowheads point to several immature vesicles, recognized by the low electron density of the insulin core. The cell-cell junctions were outlined with thin broken red lines.

(E) Density of vesicles at different stage in islets of control, $Syt4^{OE}$, or $Syt4^{-/-}$ null mouse β cells.

(F) Quantification of docked vesicles in β cells. See Figure S5 for more images used for quantification.

Error bars represent the SEM. *p < 0.05.

SYT4 Regulates Insulin Secretion in a Human β Cell Line

SYT4 is expressed in human β cells, and as in the mouse it is produced at higher levels in adult compared with fetal cells (i.e., ~3-fold [Blodgett et al., 2015]). With the objective of investigating whether *SYT4* regulates Ca^{2+}-secretion coupling in human β cells, we tested the effect of SYT4 overexpression and knockdown in human EndoC-βH1 cells. Although lentiviral vector-mediated overexpression of *SYT4* (~7-fold) had little impact on many genes' linked β cell function (e.g., *GCK, GLUT1, INSULIN, MAFA, MAFB, NEUROD1, NKX6.1, PDX1,* and *SLC30A8* [Figure 7A]), there was a significant reduction in basal insulin secretion (p = 0.04) (Figure 7B). Moreover, reducing *SYT4* levels by ~80% also had no detectable effect on the expression of most these key β cell genes, except a ~20% reduction in *INS* transcripts, in EndoC-βH1 cells (Figure 7C). Yet this knockdown significantly reduced GSIS (20 mM, p = 0.002; Figure 7D). Interestingly, this reduction in Syt4 did not increase basal insulin secretion (Figure 7D), as in *Syt4* mutant mouse islets. However, when we examined the ratio of insulin secretion at 20 mM over 2.8 mM glucose, we observed a strong trend of reduced high glucose response (p = 0.08) in SYT4 knockdown cells (Figure 7E). The implication is that, at lowered levels of SYT4, the secretable insulin vesicles had a high probability of being released at low glucose to deplete the releasable insulin vesicles, a similar conclusion as drawn in the mouse β cells. We also overexpressed SYT4 in human embryonic stem cell-derived β cells. Lentivirus-based transduction can overexpress *SYT4* in ~30% of pancreatic progenitor cells derived from human ESCs (Figure S7A). Although not statistically significant, we observed a clear trend of *SYT4* toward reduced basal insulin secretion (Figure S7B). These results suggest that the manner by which SYT4 controls insulin secretion is conserved between rodent and humans.

DISCUSSION

Calcium is the primary signal that drives β cell GSIS. Both the influx of Ca^{2+} and secretion-inducing capabilities of Ca^{2+} are optimized during β cell maturation to allow for this physiological response. However, the mechanism(s) involved in adapting to the changes in Ca^{2+} influx and Ca^{2+} signaling during β cell maturation have not been well-defined. A clearer understanding of how Ca^{2+} signaling changes during maturation has the potential to uncover post-natal β cell mechanisms that control GSIS and thus glucose homeostasis (Jacobson and Tzanakakis, 2017). Our results strongly suggest that Syt4 is involved in controlling the Ca^{2+} sensitivity of insulin vesicle secretion during β cell maturation, and Syt4 control is conserved between rodent and human β cells.

We showed that immature β cells have high insulin secretion despite similar levels of Ca^{2+} influx with mature β cells. This observation suggests that the insulin granule fusion machinery

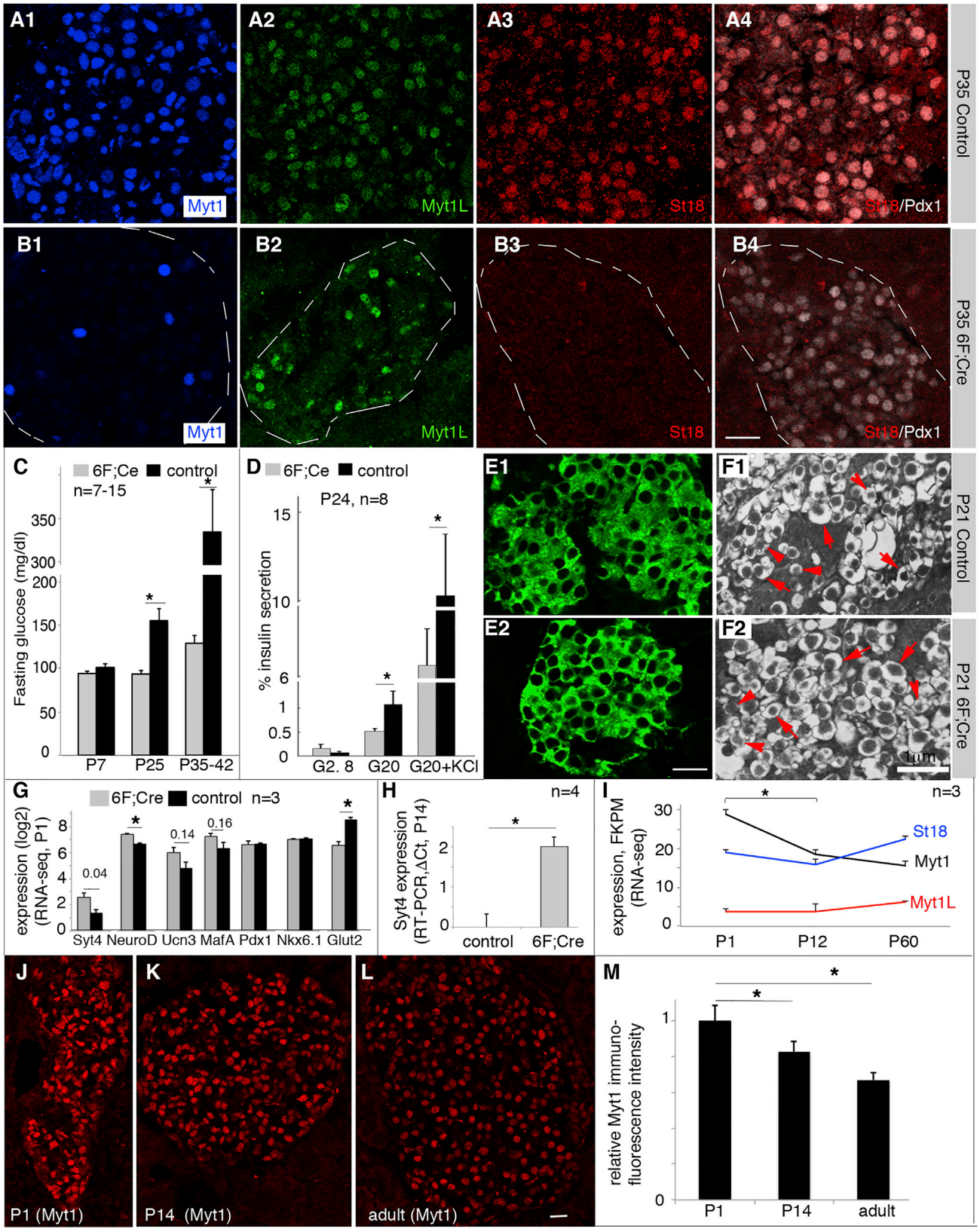

(legend on next page)

in immature β cells is more sensitive to Ca^{2+}. This sensitivity was reduced during β cell maturation. Increased production of Syt4 contributes to the regulation of this sensitivity (Figure 7F). Consistent with this model, Syt4 in neurons inhibits the ability of Syt1 to induce Ca^{2+}-dependent membrane fusion. The mechanism involves Syt4 competing with Syt1 for Syt-SNARE interactions, resulting in non-Ca^{2+} responsive Syt4-SNARE complexes due to the inability of Syt4 to bind Ca^{2+} (Bhalla et al., 2008). The primary Ca^{2+} sensor in β cells is Syt7 (Dolai et al., 2016; Gustavsson et al., 2008; Wu et al., 2015). Interestingly, we found that Syt4 and Syt7 are both localized to the insulin vesicle and non-vesicular compartments and they physically interact. Thus, one possibility is that Syt4 interacts with and modulates the ability of Syt7 to bind with SNARE components at the plasma membrane, with the levels of Syt4 inversely regulating insulin secretion (Figure 7F, top). Alternatively, Syt4 molecules localized in the ER or Golgi could interact with Syt7, which reduces vesicular levels of Syt7 and their probability of release (Figure 7F, bottom). Future sensitive assays on Syt7 levels on mature vesicles could help to resolve these possibilities.

Syt4 control of insulin secretion is further tuned by the size of the RRP of insulin vesicles in β cells. Mature β cells have a limited number of these primed insulin vesicles (Rorsman and Renström, 2003). Our data extend this concept to immature β cells, suggesting that a limited number of releasable vesicles and higher basal insulin secretion depletes these vesicles and results in poor GSIS. Consequently, when Syt4 is low and insulin granules are being secreted at low Ca^{2+} concentration, the readily releasable insulin granules pool is predicted to become depleted, accounting for the poor GSIS in immature β cells. This concept is supported by the accumulation of the RRP of vesicles following treatment of newly matured islets with glucose-free media, which promotes DSIS. Moreover, loss of *Syt4* results in an increase in the readily releasable insulin granules, suggesting that Syt4 control of insulin granule Ca^{2+} sensitivity modifies the quantity of insulin vesicles in RRP.

Interestingly, the insulin RRP decreases in *Syt4* deficient post-weaning mice, when islet GSIS demand increases with high carbohydrate diet (Stolovich-Rain et al., 2015). Along a similar line, dysfunctional islets from type II diabetic patients expressed lower levels of SYT4 (Andersson et al., 2012). These findings further imply that Syt4, in conjunction with Syt7, may have specific post-natal function in regulating vesicle biosynthesis/transport/docking during β cell maturation. Indeed, neuronal loss of *Syt4* reduces synaptic vesicle transport to the plasma membrane (Arthur et al., 2010). It will be important to determine the unique post-natal function(s) of Syt4 in trafficking and the release of the insulin granule pool with temporally controlled β cell-specific *Syt4* loss-of-function models.

It is noteworthy that, besides *Syt4*, several other non-Ca^{2+} binding *Syts* (e.g., *Syt11, 13,* and *14*) have trends or statistically significant upregulation during mouse β cell maturation (Figure S2). Interestingly, these other *Syts* are also upregulated during human β cell maturation (Blodgett et al., 2015). Thus, it is likely that these other *Syts* products can work together with Syt4 to regulate the Ca^{2+} sensitivity of insulin vesicles in a redundant fashion. Future studies to inactivate each and/or all of these *Syts* would be interesting to test their specificity and redundancy in modulating Ca^{2+}-secretion coupling in β cells.

Although increasing Syt4 limited insulin secretion in neonatal islets, high levels of Syt4 also caused compromised post-natal islet development. This may indicate that factors secreted from immature β cells control normal islet morphogenesis, islet gene expression, and proliferation. Indeed, factors packaged inside insulin vesicles such as insulin, C-peptide, insulin growth factor 2, islet amyloid polypeptide, granins, and small molecules such as GABA and ATP (Suckale and Solimena, 2010) may have autocrine effects on post-natal islet development. Particularly relevant to this possibility is the finding that mammalian target of rapamycin (mTOR) signaling can affect islet β cell maturation and islet morphogenesis (Sinagoga et al., 2017). Interfering β cell secretion with *Syt4* overexpression could interrupt these signaling processes, including mTORC2, which impairs the islet morphogenesis (Sinagoga et al., 2017). Similar examples have been proposed in other cell types, such as peptidergic nerve terminals, where changes in Syt4 levels tune neuropeptide secretion, which has been proposed to influence neuroendocrine transitions (Zhang et al., 2009). Another possibility is that intracellular Syt4 serves in regulatory capacities beyond secretion. For example, Syt4 is localized to the Golgi in many cells such as hippocampal neurons, where it plays an important role in regulating Golgi morphology in addition to synaptic vesicle formation (Arthur et al., 2010). As a substantial amount of β cell Syt4 localizes to the ER, future studies are required to examine these Syt4 effects on islet development and function; for example, by regulating the general Ca^{2+} signaling in the ER of β cells.

The regulation of *Syt4* expression remains largely unknown. Our findings suggest that Myt proteins repress *Syt4* transcription in newborn β cells, which likely prevents the detrimental effects

Figure 6. Myt Factors Repress *Syt4* Transcription

(A and B) Myt protein detection in P35 control ([con], *6F* in this case) and *6F; Cre* mutant islets. Note that A4 and B4 show examples of co-staining of St18 and Pdx1 of panels A3 and B3 to locate the islets, respectively. Scale bar, 20 μm.

(C) Fasting glucose in *6F; Cre* mutant mice (*$p \leq 0.017$).

(D) Islet GSIS and DSIS of weaned mice (P24) (*$p \leq 0.004$).

(E) Immunofluorescence to show the relative insulin level in P21 control and *6F; Cre* β cells. Scale bar, 20 μm.

(F) TEM images of insulin secretory vesicles in P21 control and *6F; Cre* β cells. Arrows, examples of mature insulin vesicles. Arrowheads, examples of immature vesicles.

(G) RNA-seq data of several genes in P1 control and *6F; Cre* β cells (n = 3). The p values (t test) of several genes were marked on the top (*$p \leq 0.041$).

(H) Real-time RT-PCR assays of *Syt4* in hand-picked P14 islets in control and *6F; Cre* islets (n = 3) (*p = 0.02).

(I) Expression levels of *Myt* genes from purified β cells (via Mip^{eGFP} expression) at different post-natal stages via RNA-seq (n = 3; *p = 0.004).

(J–M) Immunofluorescence assays of Myt1 protein levels in β cells of different ages. Wild-type (CD1) mice were used. For quantification in (M), ~200 cells were used from each stage (*$p \leq 0.04$). Scale bar, 20 μm.

Error bars represent the SEM.

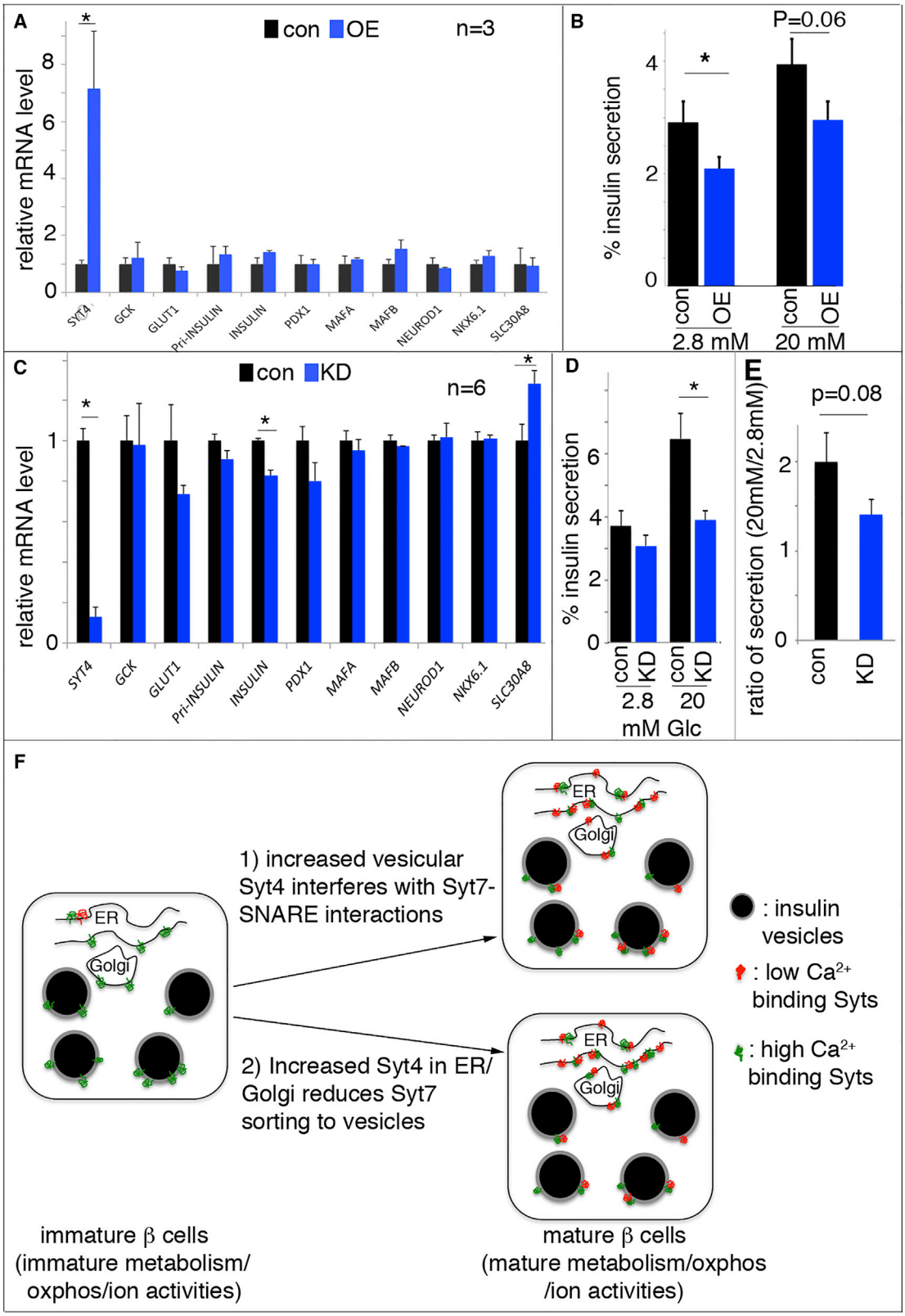

Figure 7. SYT4 Regulates Human β Cell GSIS

(A) Lentivirus was used to introduce human *SYT4* overexpression, while small interfering RNA (siRNA) were used for *SYT4* knockdown (KD). (A) Gene expression in EndoC-βH1 cells with $SYT4^{OE}$ (OE), normalized against empty virus-infected control (con) cells (*p = 0.001).

(legend continued on next page)

of precocious *Syt4* activation and β cell maturation. It is not clear, however, whether Myt factors directly repress *Syt4.* To this end, Myt1L was reported to bind the promoters of several *Syt* genes (*Syt1, 2, 3, 7,* and *12*) and to mediate their repression in fibroblasts (Mall et al., 2017). It is likely that Myts in β cells use analogous mechanisms to repress *Syt4* expression. Examining the occupancy of the *Syt4* promoter by Myts in β cells would answer this question. Also, we do not know all the factors that upregulate *Syt4* in neonatal stages. In this regard, inactivation of *MafA* does not alter *Syt4* expression (Artner et al., 2010); nor does the weaning process (data not shown). Inactivation of nuclear receptor estrogen-related receptor gamma reduces, but does not eliminate, *Syt4* expression (Yoshihara et al., 2016). Interestingly, prolactin receptor-mediated signaling, required for perinatal β cell development (Auffret et al., 2013), positively regulates *Syt4* expression (Cunha et al., 2006). Moreover, different cell types appeared to use different signals to activate *Syt4* expression. For example, diabetic conditions in humans correlated with reduced *Syt4* expression in islets (Andersson et al., 2012) but increased expression in adipose tissues (Rahimi et al., 2015). Thus, the further identification of unknown factors and mechanisms of *Syt4* expression control is needed in order to fully understand stimulus-secretion coupling in β cells.

Although both mouse and human β cell GSIS is modulated by SYT4, there are significant species-related differences in how β cells respond to *Syt4* manipulation. Inactivating *Syt4* in mouse β cells elevates basal insulin secretion; however, *SYT4* knockdown in human cells causes a trend toward lower basal insulin secretion, although the GSIS in these *SYT4* knockdown cells was even lower. It is possible that Syt4 functions differently in mouse and human cells due to the different expression profiles of different Syt paralogs in mouse and human cells. In this regard, several other *SYTs* with no/low Ca^{2+} affinity (*SYT11*, *SYT13*, *SYT14,* and *SYT16*) also displayed increased expression in maturing human β cells (Blodgett et al., 2015). They could cooperate with SYT4 to regulate Ca^{2+}-secretion coupling or other aspects of insulin vesicle biogenesis, including insulin production, packaging, and transport. It is also possible that the fetal nature of EndoC-βH1 cells impinges on SYT4 impact on basal insulin secretion. This possibility is consistent with the high expression in EndoC-βH1 cells of many markers not found in mature β cells such as HK1, HK2, and LDHA (Dhawan et al., 2015). Finally, the species-related differences in GSIS could also be due to an *in vivo* knockout occurring before birth versus an acute knockdown in a cell line. Resolving this issue requires future studies to examine the roles of different Syts in fully functional β cells from both species.

In summary, our studies reveal a previously unrecognized Syt4-mediated mechanism that regulates β cell maturation in both rodents and humans. Manipulating the Ca^{2+} sensitivity of insulin vesicles through control of *Syt4* expression, together with altering the metabolic profiles, will likely help the production of mature human β cells for transplantation-based diabetes therapy.

STAR★METHODS

Detailed methods are provided in the online version of this paper and include the following:

- KEY RESOURCES TABLE
- CONTACT FOR REAGENT AND RESOURCE SHARING
- EXPERIMENTAL MODEL AND SUBJECT DETAILS
  - Mice
  - Cell Line
- METHOD DETAILS
  - Mouse Derivation and Phenotyping
  - Glucose and Insulin Tolerance Test
  - Pancreatic Islet Isolation
  - Cell Purification, RNA-Seq-, and Real-Time PCR-Based Gene Expression Assays
  - Ca^{2+} Clamp and GSIS/DSIS Assays in Islets
  - Immunolabeling, β-Cell Mass Assays, and Electron Microscopy
  - Proximity Ligation Assays (PLA), Co-Immunoprecipitation, and Western Blotting
  - Free Cytoplasmic Ca^{2+} Recording
  - Gene Expression and GSIS Assays in Human EndoC-βH1 Cells
- QUANTIFICATION AND STATISTICAL ANALYSIS
- DATA AND SOFTWARE AVAILABILITY

SUPPLEMENTAL INFORMATION

Supplemental Information includes seven figures and two tables and can be found with this article online at https://doi.org/10.1016/j.devcel.2018.03.013.

ACKNOWLEDGMENTS

This study is supported by grants from NIDDK (DK065949 to G.G., DK089523 to M.M., DK097392 to D.A.J., DK105831 and DK108666 to M.H.) and JDRF (1-2009-371 to G.G.). Confocal and TEM imaging were performed with VUMC Cell Imaging Shared Resource (supported by NIH grants CA68485, DK20593, DK58404, DK59637, and EY08126).

(B) GSIS in EndoC-βH1 cells with $SYT4^{OE}$ (*p = 0.04).
(C) Gene expression in EndoC-βH1 cells with $SYT4^{KD}$ (KD), normalized against cells treated with scrabbled siRNA (con) (*p ≤ 0.02).
(D and E) Insulin secretion in EndoC-βH1 cells with $SYT4^{KD}$, presented as the percentage of insulin secretion at different level of glucose (D), or as the ratio of insulin release at 20 mM over 2.8 mM glucose (E) (*p = 0.02).
(F) A model with two pathways that converge to regulate β cell maturation: one aspect includes glucose metabolism/subsequent oxidative phosphorylation and membrane excitability, which ensure efficient glucose metabolism, ATP production, ionic activity, and Ca^{2+} entry. Another is the modulation of Ca^{2+} sensitivity of the vesicles. In this pathway, immature β cells have lower levels and mature β cells have higher levels of non-Ca^{2+}-binding Syts. The Ca^{2+}-binding Syts remain unchanged during maturation. The increased ratio between non-Ca^{2+}- to Ca^{2+}-binding Syts can desensitize the vesicles so that high secretion only occurs at high Ca^{2+} in the mature β cells. This desensitization can be achieved by (1) using Syt4 localized on vesicles to inhibit Syt7-SNARE interactions, (2) reducing Syt7 levels on vesicle surface, or both.
Error bars represent the SEM.

AUTHOR CONTRIBUTIONS

G.G., M.G., D.A.J., M.A.M., and C.J.S. conceptualized the work and designed the experiments. C.H., G.G., R.H., Y.X., and W.Z. did gene expression and secretion assays in mice. Y.X. and S.W. derived the conditional Myt gene alleles and examined mutant phenotypes. P.K.D. recorded Ca^{2+} responses in islets. J.L., G.G.N., and M.H. performed and discussed Syt4 function in human ESC-derived β cells. E.M.W. and R.S. did analysis in human β cell lines. J.W. did TEM imaging. J.M. analyzed the TEM images and helped with islet isolation. T.S. did bioinformatics data processing and deposition. W.H. and A.T.H.Y. provided $Syt7^{-/-}$ pancreata. All authors participated in manuscript preparation and editing.

DECLARATION OF INTERESTS

The authors declare no competing interests.

Received: September 28, 2017
Revised: February 12, 2018
Accepted: March 19, 2018
Published: April 12, 2018

REFERENCES

Aguayo-Mazzucato, C., Zavacki, A.M., Marinelarena, A., Hollister-Lock, J., El Khattabi, I., Marsili, A., Weir, G.C., Sharma, A., Larsen, P.R., and Bonner-Weir, S. (2013). Thyroid hormone promotes postnatal rat pancreatic beta-cell development and glucose-responsive insulin secretion through MAFA. Diabetes *62*, 1569–1580.

Ammälä, C., Ashcroft, F.M., and Rorsman, P. (1993). Calcium-independent potentiation of insulin release by cyclic AMP in single beta-cells. Nature *363*, 356–358.

Andersson, S.A., Olsson, A.H., Esguerra, J.L., Heimann, E., Ladenvall, C., Edlund, A., Salehi, A., Taneera, J., Degerman, E., Groop, L., et al. (2012). Reduced insulin secretion correlates with decreased expression of exocytotic genes in pancreatic islets from patients with type 2 diabetes. Mol. Cell. Endocrinol. *364*, 36–45.

Arthur, C.P., Dean, C., Pagratis, M., Chapman, E.R., and Stowell, M.H. (2010). Loss of synaptotagmin IV results in a reduction in synaptic vesicles and a distortion of the Golgi structure in cultured hippocampal neurons. Neuroscience *167*, 135–142.

Artner, I., Hang, Y., Mazur, M., Yamamoto, T., Guo, M., Lindner, J., Magnuson, M.A., and Stein, R. (2010). MafA and MafB regulate genes critical to beta-cells in a unique temporal manner. Diabetes *59*, 2530–2539.

Auffret, J., Freemark, M., Carre, N., Mathieu, Y., Tourrel-Cuzin, C., Lombes, M., Movassat, J., and Binart, N. (2013). Defective prolactin signaling impairs pancreatic beta-cell development during the perinatal period. Am. J. Physiol. Endocrinol. Metab. *305*, E1309–E1318.

Berton, F., Cornet, V., Iborra, C., Garrido, J., Dargent, B., Fukuda, M., Seagar, M., and Marqueze, B. (2000). Synaptotagmin I and IV define distinct populations of neuronal transport vesicles. Eur. J. Neurosci. *12*, 1294–1302.

Bhalla, A., Chicka, M.C., and Chapman, E.R. (2008). Analysis of the synaptotagmin family during reconstituted membrane fusion. Uncovering a class of inhibitory isoforms. J. Biol. Chem. *283*, 21799–21807.

Blodgett, D.M., Nowosielska, A., Afik, S., Pechhold, S., Cura, A.J., Kennedy, N.J., Kim, S., Kucukural, A., Davis, R.J., Kent, S.C., et al. (2015). Novel observations from next-generation RNA sequencing of highly purified human adult and fetal islet cell subsets. Diabetes *64*, 3172–3181.

Blum, B., Hrvatin, S., Schuetz, C., Bonal, C., Rezania, A., and Melton, D.A. (2012). Functional beta-cell maturation is marked by an increased glucose threshold and by expression of urocortin 3. Nat. Biotechnol. *30*, 261–264.

Brouwers, B., de Faudeur, G., Osipovich, A.B., Goyvaerts, L., Lemaire, K., Boesmans, L., Cauwelier, E.J., Granvik, M., Pruniau, V.P., Van Lommel, L., et al. (2014). Impaired islet function in commonly used transgenic mouse lines due to human growth hormone minigene expression. Cell Metab. *20*, 979–990.

Craxton, M. (2004). Synaptotagmin gene content of the sequenced genomes. BMC Genomics *5*, 43.

Cunha, D.A., Amaral, M.E., Carvalho, C.P., Collares-Buzato, C.B., Carneiro, E.M., and Boschero, A.C. (2006). Increased expression of SNARE proteins and synaptotagmin IV in islets from pregnant rats and in vitro prolactin-treated neonatal islets. Biol. Res. *39*, 555–566.

Dean, C., Liu, H., Dunning, F.M., Chang, P.Y., Jackson, M.B., and Chapman, E.R. (2009). Synaptotagmin-IV modulates synaptic function and long-term potentiation by regulating BDNF release. Nat. Neurosci. *12*, 767–776.

Dhawan, S., Tschen, S.I., Zeng, C., Guo, T., Hebrok, M., Matveyenko, A., and Bhushan, A. (2015). DNA methylation directs functional maturation of pancreatic beta cells. J. Clin. Invest. *125*, 2851–2860.

Do, O.H., Low, J.T., Gaisano, H.Y., and Thorn, P. (2014). The secretory deficit in islets from db/db mice is mainly due to a loss of responding beta cells. Diabetologia *57*, 1400–1409.

Dolai, S., Xie, L., Zhu, D., Liang, T., Qin, T., Xie, H., Kang, Y., Chapman, E.R., and Gaisano, H.Y. (2016). Synaptotagmin-7 functions to replenish insulin granules for exocytosis in human islet beta-cells. Diabetes *65*, 1962–1976.

Fukuda, M., Kanno, E., Ogata, Y., Saegusa, C., Kim, T., Loh, Y.P., and Yamamoto, A. (2003). Nerve growth factor-dependent sorting of synaptotagmin IV protein to mature dense-core vesicles that undergo calcium-dependent exocytosis in PC12 cells. J. Biol. Chem. *278*, 3220–3226.

Goodyer, W.R., Gu, X., Liu, Y., Bottino, R., Crabtree, G.R., and Kim, S.K. (2012). Neonatal beta cell development in mice and humans is regulated by calcineurin/NFAT. Dev. Cell *23*, 21–34.

Grasso, S., Messina, A., Saporito, N., and Reitano, G. (1968). Serum-insulin response to glucose and aminoacids in the premature infant. Lancet *2*, 755–756.

Grynkiewicz, G., Poenie, M., and Tsien, R.Y. (1985). A new generation of Ca^{2+} indicators with greatly improved fluorescence properties. J. Biol. Chem. *260*, 3440–3450.

Gu, C., Stein, G.H., Pan, N., Goebbels, S., Hornberg, H., Nave, K.A., Herrera, P., White, P., Kaestner, K.H., Sussel, L., et al. (2010). Pancreatic beta cells require NeuroD to achieve and maintain functional maturity. Cell Metab. *11*, 298–310.

Gu, G., Wells, J.M., Dombkowski, D., Preffer, F., Aronow, B., and Melton, D.A. (2004). Global expression analysis of gene regulatory pathways during endocrine pancreatic development. Development *131*, 165–179.

Gustavsson, N., Lao, Y., Maximov, A., Chuang, J.C., Kostromina, E., Repa, J.J., Li, C., Radda, G.K., Sudhof, T.C., and Han, W. (2008). Impaired insulin secretion and glucose intolerance in synaptotagmin-7 null mutant mice. Proc. Natl. Acad. Sci. USA *105*, 3992–3997.

Hang, Y., and Stein, R. (2011). MafA and MafB activity in pancreatic beta cells. Trends Endocrinol. Metab. *22*, 364–373.

Huang, C., and Gu, G. (2017). Effective isolation of functional islets from neonatal mouse pancreas. J. Vis. Exp. https://doi.org/10.3791/55160.

Jacobson, D.A., Mendez, F., Thompson, M., Torres, J., Cochet, O., and Philipson, L.H. (2010). Calcium-activated and voltage-gated potassium channels of the pancreatic islet impart distinct and complementary roles during secretagogue induced electrical responses. J. Physiol. *588*, 3525–3537.

Jacobson, E.F., and Tzanakakis, E.S. (2017). Human pluripotent stem cell differentiation to functional pancreatic cells for diabetes therapies: innovations, challenges and future directions. J. Biol. Eng. *11*, 21.

Jacovetti, C., Matkovich, S.J., Rodriguez-Trejo, A., Guay, C., and Regazzi, R. (2015). Postnatal beta-cell maturation is associated with islet-specific microRNA changes induced by nutrient shifts at weaning. Nat. Commun. *6*, 8084.

Jermendy, A., Toschi, E., Aye, T., Koh, A., Aguayo-Mazzucato, C., Sharma, A., Weir, G.C., Sgroi, D., and Bonner-Weir, S. (2011). Rat neonatal beta cells lack the specialised metabolic phenotype of mature beta cells. Diabetologia *54*, 594–604.

Johnson, S.L., Franz, C., Kuhn, S., Furness, D.N., Rüttiger, L., Munkner, S., Rivolta, M.N., Seward, E.P., Herschman, H.R., Engel, J., et al. (2010).

Synaptotagmin IV determines the linear Ca2+ dependence of vesicle fusion at auditory ribbon synapses. Nat. Neurosci. *13*, 45–52.

Kalwat, M.A., and Cobb, M.H. (2017). Mechanisms of the amplifying pathway of insulin secretion in the beta cell. Pharmacol. Ther. *179*, 17–30.

Kieffer, T.J. (2016). Closing in on mass production of mature human beta cells. Cell Stem Cell *18*, 699–702.

Lemaire, K., Thorrez, L., and Schuit, F. (2016). Disallowed and allowed gene expression: two faces of mature islet beta cells. Annu. Rev. Nutr. *36*, 45–71.

Littleton, J.T., Serano, T.L., Rubin, G.M., Ganetzky, B., and Chapman, E.R. (1999). Synaptic function modulated by changes in the ratio of synaptotagmin I and IV. Nature *400*, 757–760.

Liu, J.S., and Hebrok, M. (2017). All mixed up: defining roles for beta-cell subtypes in mature islets. Genes Dev. *31*, 228–240.

Machado, H.B., Liu, W., Vician, L.J., and Herschman, H.R. (2004). Synaptotagmin IV overexpression inhibits depolarization-induced exocytosis in PC12 cells. J. Neurosci. Res. *76*, 334–341.

Mall, M., Kareta, M.S., Chanda, S., Ahlenius, H., Perotti, N., Zhou, B., Grieder, S.D., Ge, X., Drake, S., Euong Ang, C., et al. (2017). Myt1l safeguards neuronal identity by actively repressing many non-neuronal fates. Nature *544*, 245–249.

Moore-Dotson, J.M., Papke, J.B., and Harkins, A.B. (2010). Upregulation of synaptotagmin IV inhibits transmitter release in PC12 cells with targeted synaptotagmin I knockdown. BMC Neurosci. *11*, 104.

Nishimura, W., Kondo, T., Salameh, T., El Khattabi, I., Dodge, R., Bonner-Weir, S., and Sharma, A. (2006). A switch from MafB to MafA expression accompanies differentiation to pancreatic beta-cells. Dev. Biol. *293*, 526–539.

Osterberg, J.R., Chon, N.L., Boo, A., Maynard, F.A., Lin, H., and Knight, J.D. (2015). Membrane docking of the synaptotagmin 7 C2A domain: electron paramagnetic resonance measurements show contributions from two membrane binding loops. Biochemistry *54*, 5684–5695.

Pildes, R.S., Hart, R.J., Warrner, R., and Cornblath, M. (1969). Plasma insulin response during oral glucose tolerance tests in newborns of normal and gestational diabetic mothers. Pediatrics *44*, 76–83.

Rahimi, M., Vinciguerra, M., Daghighi, M., Özcan, B., Akbarkhanzadeh, V., Sheedfar, F., Amini, M., Mazza, T., Pazienza, V., Motazacker, M.M., et al. (2015). Age-related obesity and type 2 diabetes dysregulate neuronal associated genes and proteins in humans. Oncotarget *6*, 29818–29832.

Ravassard, P., Hazhouz, Y., Pechberty, S., Bricout-Neveu, E., Armanet, M., Czernichow, P., and Scharfmann, R. (2011). A genetically engineered human pancreatic beta cell line exhibiting glucose-inducible insulin secretion. J. Clin. Invest. *121*, 3589–3597.

Rorsman, P., Arkhammar, P., Bokvist, K., Hellerström, C., Nilsson, T., Welsh, M., Welsh, N., and Berggren, P.O. (1989). Failure of glucose to elicit a normal secretory response in fetal pancreatic beta cells results from glucose insensitivity of the ATP-regulated K+ channels. Proc. Natl. Acad. Sci. USA *86*, 4505–4509.

Rorsman, P., and Renström, E. (2003). Insulin granule dynamics in pancreatic beta cells. Diabetologia *46*, 1029–1045.

Rozzo, A., Meneghel-Rozzo, T., Delakorda, S.L., Yang, S.B., and Rupnik, M. (2009). Exocytosis of insulin: in vivo maturation of mouse endocrine pancreas. Ann. N. Y. Acad. Sci. *1152*, 53–62.

Scarlett, J.M., and Schwartz, M.W. (2015). Gut-brain mechanisms controlling glucose homeostasis. F1000Prime Rep. *7*, 12.

Sinagoga, K.L., Stone, W.J., Schiesser, J.V., Schweitzer, J.I., Sampson, L., Zheng, Y., and Wells, J.M. (2017). Distinct roles for the mTOR pathway in postnatal morphogenesis, maturation and function of pancreatic islets. Development *144*, 2402–2414.

Stolovich-Rain, M., Enk, J., Vikesa, J., Nielsen, F.C., Saada, A., Glaser, B., and Dor, Y. (2015). Weaning triggers a maturation step of pancreatic beta cells. Dev. Cell *32*, 535–545.

Suckale, J., and Solimena, M. (2010). The insulin secretory granule as a signaling hub. Trends Endocrinol. Metab. *21*, 599–609.

Südhof, T.C. (2012). The presynaptic active zone. Neuron *75*, 11–25.

Thomas, D.M., Ferguson, G.D., Herschman, H.R., and Elferink, L.A. (1999). Functional and biochemical analysis of the C2 domains of synaptotagmin IV. Mol. Biol. Cell *10*, 2285–2295.

Trapnell, C., Roberts, A., Goff, L., Pertea, G., Kim, D., Kelley, D.R., Pimentel, H., Salzberg, S.L., Rinn, J.L., and Pachter, L. (2012). Differential gene and transcript expression analysis of RNA-seq experiments with TopHat and Cufflinks. Nat. Protoc. *7*, 562–578.

van der Meulen, T., Donaldson, C.J., Cáceres, E., Hunter, A.E., Cowing-Zitron, C., Pound, L.D., Adams, M.W., Zembrzycki, A., Grove, K.L., and Huising, M.O. (2015). Urocortin3 mediates somatostatin-dependent negative feedback control of insulin secretion. Nat. Med. *21*, 769–776.

Wang, S., Yan, J., Anderson, D.A., Xu, Y., Kanal, M.C., Cao, Z., Wright, C.V., and Gu, G. (2010). Neurog3 gene dosage regulates allocation of endocrine and exocrine cell fates in the developing mouse pancreas. Dev. Biol. *339*, 26–37.

Wang, S., Zhang, J., Zhao, A., Hipkens, S., Magnuson, M.A., and Gu, G. (2007). Loss of Myt1 function partially compromises endocrine islet cell differentiation and pancreatic physiological function in the mouse. Mech. Dev. *124*, 898–910.

Warming, S., Costantino, N., Court, D.L., Jenkins, N.A., and Copeland, N.G. (2005). Simple and highly efficient BAC recombineering using galK selection. Nucleic Acids Res. *33*, e36.

Wu, B., Wei, S., Petersen, N., Ali, Y., Wang, X., Bacaj, T., Rorsman, P., Hong, W., Sudhof, T.C., and Han, W. (2015). Synaptotagmin-7 phosphorylation mediates GLP-1-dependent potentiation of insulin secretion from beta-cells. Proc. Natl. Acad. Sci. USA *112*, 9996–10001.

Yoshihara, E., Wei, Z., Lin, C.S., Fang, S., Ahmadian, M., Kida, Y., Tseng, T., Dai, Y., Yu, R.T., Liddle, C., et al. (2016). ERRgamma is required for the metabolic maturation of therapeutically functional glucose-responsive beta cells. Cell Metab. *23*, 622–634.

Zhang, Z., Bhalla, A., Dean, C., Chapman, E.R., and Jackson, M.B. (2009). Synaptotagmin IV: a multifunctional regulator of peptidergic nerve terminals. Nat. Neurosci. *12*, 163–171.

Zhao, A., Ohara-Imaizumi, M., Brissova, M., Benninger, R.K., Xu, Y., Hao, Y., Abramowitz, J., Boulay, G., Powers, A.C., Piston, D., et al. (2010). Galphao represses insulin secretion by reducing vesicular docking in pancreatic beta-cells. Diabetes *59*, 2522–2529.

Zhu, X., Hu, R., Brissova, M., Stein, R.W., Powers, A.C., Gu, G., and Kaverina, I. (2015). Microtubules negatively regulate insulin secretion in pancreatic beta cells. Dev. Cell *34*, 656–668.

STAR★METHODS

KEY RESOURCES TABLE

REAGENT or RESOURCE	SOURCE	IDENTIFIER
Antibodies		
488-donkey anti Guinea Pig	Jackson Immunoresearch	CAT# 706-545-148; RRID:AB_234472
488-donkey anti goat igG	Jackson Immunoresearch	CaT# 705-545-147; RRID:AB_2336933
Alexa Fluor® 647 AffiniPure Donkey Anti-Guinea Pig IgG (H+L)	Jackson Immunoresearch	CAT# 706-605-148; RRID:AB_2340476
Alexa Fluor® 488 AffiniPure Donkey Anti-Rabbit IgG (H+L)	Jackson Immunoresearch	CAT# 711-545-152; RRID:AB_2313584
Alexa Fluor® 647 AffiniPure Donkey Anti-Rabbit	Jackson Immunoresearch	CAT# 711-605-152: RRID:AB_2492288
Alexa Fluor® 647 AffiniPure Donkey Anti-Mouse IgG (H+L)	Jackson Immunoresearch	CAT# 715-605-150; RRID:AB_2340862
Alexa Fluor® 594 AffiniPure Donkey Anti-Mouse	Jackson Immunoresearch	CAT# 715-585-150; RRID:AB_2340584
Alexa Fluor® 594 AffiniPure Donkey Anti-Goat IgG (H+L)	Jackson Immunoresearch	CAT# 705-585-003; RRID:AB_2340432
Alexa 647 AffiniPure Rabbit Anti-Syrian Hamster IgG (H+L)	Jackson Immunoresearch	CAT# 307-605-003; RRID:AB_2339601
Biotin-sp anti rabbit	Jackson Immunoresearch	CAT# 711065-152; RRID:AB_2340593
biotin anti Rat	Jackson Immunoresearch	712-065-151
Cy3-Donkey anti-mouse	Jackson Immunoreserach	CAT# 715-165-150; RRID:AB_2340813
Cy3-streptavidin	Vector laboroatories	SA-1300
Cy5- streptavidin	Vector laboroatories	SA-1500
FITC anti Rabbit	Jackson Immunoresearch	CAT# 711-095-152; RRID:AB_2315776
Goat anti-Pdx1	ABcam	CAT# AB47383; RRID:AB_2162359
Goat anti-somatostatin	ABcam	CAT# AB30788; RRID:AB_778010
Goat anti-insulin	Santa Cruz	sc-7839
Guinea pig anti Myt1L	This paper	N/A
Guinea pig anti insulin	Dako	A0564
Mouse anti-Syt4	Abcam	CAT# Ab57473; RRID:AB_945716
Mouse anti glucagon	Millipore	MabN238
Mouse anti-GM130	LS BioSciences	LS-C482425
Mouse anti-HA-conjugated beads	Vanderbilt Antibody/Protein Resource	N/A
Rabbit anti-Pdx1	ABcam	CAT# AB47267; RRID:AB_1503594
Rabbit anti-Nkx6.1	Gift of P. Serup	N/A
Rabbit anti MafA	Novus	CAT# NBP1-00121; RRID:AB_1503594
Rabbit anti-Syt4	SYSY	CAT# 105043; RRID:AB_887837
Rabbit anti-Syt7	SYSY	CAT# 105173; RRID:AB_887838
Rabbit anti-PDI	Cell signaling	CAT# 2446S; RRID:AB_2298935
Rabbit anti-Myt1	This laboratory	N/A
Rabbit anti-glucagon	ABcam	CAT# AB92517; RRID:AB_10561971
Rabbit anti-HA	Cell signaling	#3724
Rabbit anti-somatostatin	ABcam	CAT# AB6741; RRID:AB_955424
Rabbit anti-Ki67	Abcam	CAT# Ab 15580; RRID:AB_443209
Rabbit anti-Glut2	Alpha Diagnostic	CAT# GT21-A: RRID:AB_1616640
Rabbit anti-MafB	Gift of R. Stein	N/A
Rat anti St18	This paper	N/A
Bacterial and Virus Strains		
Bl-21	Vanderbilt MPB Core	N/A
DH5-alpha	Vanderbilt MPB Core	N/A

(*Continued on next page*)

Continued

REAGENT or RESOURCE	SOURCE	IDENTIFIER
Multiple Lentiviral Expression System Kit	Addgene	Kit #1000000060
XI-1	Vanderbilt MPB Core	N/A
Biological Samples		
Bovine serum albumin	Sigma	A9418
Donkey Serum	Jackson Immunoresearch	017-000-121
Fetal Bovine Serum	Atlanta Biologicals	S10250
Lenti virus-SYT4	This paper	N/A
SYT4 siRNA mix	GE healthCare	MHS6278-202807867
Chemicals, Peptides, and Recombinant Proteins		
Collagenase from Clostridium histolyticum	Sigma	C5138
DMSO	Sigma	D2650
Doxycycline	Sigma	D9891
HBSS-with Ca^{2+}/Mg2+	Mediatech	20-020-CV
HBSS-without Ca^{2+}/Mg2+	Mediatech	20-021-CV
IBMX	WAKO	095-03413
Ionomycin	Sigma	407953
HistoClear	FisherScientific	HS2001GLL
Human fibronectin	Sigma	TR-1003-G
paraformaldehyde	Sigma	P6148
Polybrene	Sigma	TR-1003
Protease inhibitors	ThermoFisher	88665
RNAiMax	ThermoFisher	13778030
Trypsin	Sigma	C5138-5G
Critical Commercial Assays		
Elisa Insulin kit	Alpco	80-INSUMSU-E01
Ca^{2+} calibration kit	ThermoFisher	F6774
High capacity cDNA synthesis	Applied BIosystems	4368814
Magnetic beads conjugated with anti-HA	Vanderbilt Antibody and Protein Resource	N/A
PLA kit	Sigma Aldrich	DUO92101
SYBER Green qpcr mix	Biorad	1705060
Deposited Data		
RNAseq-P1 β cells	1998-GG-2	ArrayExpress: E-MTAB-2266
RNAseq-P1 β cells	1998-GG-3	ArrayExpress: E-MTAB-2266
RNAseq-P1 β cells	1998-GG-4	ArrayExpress: E-MTAB-2266
RNAseq-P12 β cells	1998-GG-8	ArrayExpress: E-MTAB-2266
RNAseq-P12 β cells	1998-GG-9	ArrayExpress: E-MTAB-2266
RNAseq-P12 β cells	1998-GG-10	ArrayExpress: E-MTAB-2266
RNAseq-P60 β cells	1998-GG-28	ArrayExpress: E-MTAB-2266
RNAseq-P60 β cells	1998-GG-29	ArrayExpress: E-MTAB-2266
RNAseq-P60 β cells	1998-GG-30	ArrayExpress: E-MTAB-2266
RNAseq-P1 Myt mutant β cells	1949-GG-42	ArrayExpress: E-MTAB-6615
RNAseq-P1 Myt mutant β cells	1949-GG-43	ArrayExpress: E-MTAB-6615
RNAseq-P1 Myt mutant β cells	2687-GG-14	ArrayExpress: E-MTAB-6615
Experimental Models: Cell Lines		
EndoC-βH1	Gift of Scharfmann	N/A
HEK293T	ATCC	CRL-1573TM

CONTACT FOR REAGENT AND RESOURCE SHARING

Further information and requests for resources and reagents may be directed to and will be fulfilled by the Lead Contact, Guoqiang Gu (guoqiang.gu@vanderbilt.edu).

EXPERIMENTAL MODEL AND SUBJECT DETAILS

Mice

Mouse usage conforms to protocols approved by the Vanderbilt University IACUC for Dr. Gu, in compliance with regulations of AAALAC. All mice were housed in a level 6 facility, in a particular room that has no detectable pathogens. Mice are housed in 51-squre inch ages, with have autoclaved hard-wood derived bedding and *ad lib* access to water and chew. For new born mice, one litter will be housed in each cage. For post weaning mice (genotyped around day 14-20), a maximum of 5 mice of same sex were housed. For husbandry, one male mouse was housed together with two females of breeding age until cross. Plugs were checked daily to identify plugged females, which were transferred to new cages for birth.

Wild-type CD1 (ICR) mice were from Charles River Laboratories. *Flipe*, Rip^{rtTA} and $Syt4^{+/-}$ mice were from the Jackson Laboratories. $Rip^{mCherry}$ mice were derived in Vanderbilt Transgenic Mouse/ES Cell Shared Resource and reported in (Zhu et al., 2015). The $TetO^{Syt4}$, $Myt1L^{F}$, and $St18^{F}$ mice were derived in Vanderbilt as well.

Cell Line

HEK293T. These cells were isolated from a female human embryonic kidney (HEK), transformed with large T antigen.

METHOD DETAILS

Mouse Derivation and Phenotyping

$TetO^{Syt4}$ mice were derived by pronuclear injection with a DNA construct made by ligating a TetO-CMV promoter (PTRE2, Clontech), the *Syt4* coding sequence, and a SV40 polyA signal. The DNA construct was verified by sequencing. Three independent lines were derived, all without recognizable defects. For *Syt4* over expression, doxycycline (2 mg/ml) was added to the drinking water of pregnant mice from E16.5 until P10 or to the time of tissue collection (if tissue collection was before P10). Both male and female mice were included for all studies, with similar numbers of both sexes.

$Myt1L^{F}$ and $St18^{F}$ derivation used routine targeting (Figure S6). Briefly, BAC clones RP22-191C21 and RP22-214C11 were used to isolate *Myt1L* and *St18* genomic fragments via BAC recombineering (Warming et al., 2005). Targeting vectors were made so that the exons 12+13 in Myt1L (coding amino acid residues 491-566) and exons 9+10 in St18 (coding amino acid resides 355-429) were flanked with LoxP sites (Figure S6). Such designs introduced frame shifts in *Myt1L* and *St18* mRNAs after Cre-mediated recombination. The homologous recombination arms were 7.2/2.6 kb for *Myt1L* and 3.1/8.2 kb for *St18*. Properly targeted TL1 (male) ES cell clones were verified by southern blots on both 5' and 3' probes. After chimera production and selection cassette removal with *Flipe* mice, PCR were used for genotyping (with DNA oligos listed in Table S2).

The functionality of the $Myt1L^{F}$ and $St18^{F}$ alleles were authenticated by producing $Myt1L^{F/F}$, $St18^{F/F}$, $Myt1L^{F/F}$; *Pdx1Cre*, and $St18^{F/F}$; *Pdx1Cre* mice. None of these mice have detectable phenotypes. For unknown reasons that might be related with nonsense-mediated degradation or protein instability, the $Myt1L^{F/F}$; *Pdx1Cre*, and $St18^{F/F}$; *Pdx1Cre* islets did not produce detectable N-terminal Myt1L or St18 protein fragments, which were expected to be translated from mRNAs transcribed from the $Myt1L^{-}$ and $St18^{-}$ alleles after Cre-mediated recombination. The newly derived Myt1L and St18 antibodies used in this study were raised using antigens localized to the N-terminal side of the deleted protein region (see information about Myt1L and St18 antibody derivation and Figure 6B).

Glucose and Insulin Tolerance Test

For IPGTT, and ITT, mice were fasted overnight or 4 hours, respectively. Glucose or insulin was injected at 2mg/kg or 1 unit/kg via intraperitoneal injection, respectively. Blood glucose was then measured via tail snip at the time points indicated in the manuscript. For serum insulin assays, whole blood was collected via retro-orbital bleeding into EDTA-coated tubes. Plasma were then prepared by centrifugation and used for down stream assays.

Pancreatic Islet Isolation

Pancreata were directly digested (for P1 and P12 pancreata) (Huang and Gu, 2017) or perfused (for pancreata older than 2 weeks) (Zhao et al., 2010) with 0.5 mg/ml Type IV collagenase dissolved in Hanks Balanced Salt Solution (HBSS) with Ca^{2+}/Mg^{2+}. After digestion at 37°C, lysates were washed in RPMI 1640 with 5.6 mM glucose and 10% fetal bovine serum (i.e. RPMIFBS) for 4 times. Islets were handpicked for down stream usage.

Cell Purification, RNA-Seq-, and Real-Time PCR-Based Gene Expression Assays

Handpicked Mip^{eGFP} or $Rip^{mcherry}$ islets were washed in HBSS without Ca^{2+}/Mg^{2+} for 5 minutes and dissociated into single cells with 0.25% trypsin at 37°C as in (Gu et al., 2004). The dissociation usually lasted for less than 10 minutes. Cells were pipetted once every

2 minutes to aide dissociation. When ~half of the cells appeared as singles, the digestion was stopped by washing with RPMIFBS 3 times in 1.5 ml tubes. Cells were then filtered, stained with propidium iodide, and sorted using a BD FACSAria III cell sorter. Live/single/fluorescence+ cells were collected and verified under microscopes. *Mip*^{eGFP} mice express human growth hormone (hGH), which can impact the expression of some genes (Brouwers et al., 2014), while *Rip*^{mcherry} mice have no *hGH* sequence.

For RNA-seq, RNA was prepared with TRIzol (Life Technologies) and a DNA free RNA^{TM} kit following manufacturer's protocols (Zymo Research). 200 ng total RNAs with RINs above 8 (assessed using Agilent Bioanalyzer 2100) were sequenced, with 3 biological replicas for each stage/genotype, following Illumina protocols on HiSeq-2000. Raw reads were processed and analyzed with TopHat and Cufflinks to determine the relative abundance of gene expression at each stages, reported as FPKM (Fragments Per Kilobase of transcript per Million mapped reads) (Trapnell et al., 2012). Real time RT-PCR utilized SYBR green master mix of the Bio-Rad system, with oligos listed in Table S2.

Ca^{2+} Clamp and GSIS/DSIS Assays in Islets

Secretion was assayed with the % of total insulin secreted within a 45-minute time window, unless noted. Hand-picked islets were allowed to recover in RPMIFBS for ~2 hours or overnight. Islets were washed twice with pre-warmed KRB solution (2.8 mM glucose, 102 mM NaCl, 5 mM KCl, 1.2 mM MgCl2, 2.7 mM CaCl2, 20 mM HEPES, 5 mM NaHCO3, and 10 mg/ml BSA, pH 7.4). Islets were then incubated in KRB (37°C) for one hour, washed with pre-warmed KRB once again. ~10 islet were then transferred into each wells of 12-well plates with 1 ml pre-warmed KRB to start the secretion assays. For ionomycin-mediated Ca^{2+} clamp, hand-picked islets were pre-incubated with 0.25 mM diazoxide for one hour. 50 μM ionomycin was then added to induce insulin secretion. For all assays, at least six mice of each genotype were used for islet isolation, with islets from two or more mice examined in each independent experiment (as three-four technical replicas).

Insulin was assayed with Elisa kit from Alpco following manufacturer protocol. For assaying insulin per cell, specific numbers of sorted cells were directly extracted with ethanol-HCl for total insulin quantification (Zhao et al., 2010).

Immunolabeling, β-Cell Mass Assays, and Electron Microscopy

Immunoflorescence staining followed published procedures (Wang et al., 2007, 2010) with antibodies in the Key Resources Table. Briefly, tissue sections or cells attached on slides were washed in 1XPhosphate Buffered Saline (PBS) 3 time, 5 minutes each. The frozen sections were permeabilized in basal staining buffer (1XPBS+ 0.1% triton X100 + 0.1% Tween-20) for 30 minutes at room temperature (slides from paraffin embedded tissues did need permeabilization). Samples were blocked with blocking buffer (1XPBS+ 0.1% triton X100 + 0.1% Tween-20 + 0.1% BSA + 0.05% donkey serum, 100 micro-litter per slide) for another 30 minutes at room temperature. Primary antibodies (100 micro-litter per slide) diluted in blocking buffer were then added (see below for dilution) and incubate at 4°C overnight. After three time wash in basal staining buffer, secondary antibodies diluted in blocking buffer were overlaid on slides (100 micro litter each slide), incubate for 1 hour at room temperature, washed three times with basal buffer, and mounted for observation. All primary and secondary antibodies except that against Syt4 (1:200 dilution) and Syt7 (1:500 dilution) used 1:1000 dilutions.

For hormones and transcription factor staining, frozen or paraffin tissue sections were both used. Tissue section preparations followed routine procedures: pancreata were dissected; large pancreata (older than P14) were cut into 5-10 small pieces and fixed in 4% paraformaldehyde overnight at 4°C; fixed tissues were washed with PBS 3 times (10 minutes each) and prepared for frozen or paraffin blocks (following dehydration through PBS, 40%, 70%, 85%, 100% ethanol, and HistoClear; 15 and 6 μm thick sections were prepared for frozen and paraffin sections, respectively. For antibodies against Syt4, Syt7, GM130, and PDI, islet cells attached to glass coverslips were used. For Syt4 quantification, post-fixation (after freshly isolated islets were partially dissociated and attached onto slides with cytospin) was used, which appeared to produce better dynamic range of immunofluorescence signals. For subcellular localization, islets were isolated and partially dissociated into small cell clusters (~5-20 cells per cluster) with trypsin. Cells were then cultured on glass coverslips coated with human fibronectin in RPMIFBS. After 24 hours, samples were fixed in 4% paraformaldehyde for 15 minutes and processed for immunolabeling. Paraffin sections were de-waxed through HistoClear, 100%, 85%, 70%, 40% ethanol, and PBS solutions for antibody staining.

For co-labeling with antibodies raised in the same host (amongst PDI, Syt4, and Syt7), one round of labeling would be completed first with proper fluorophore-conjugated secondary antibodies. The samples were blocked with anti-IgG of the host, followed by routine labeling for the second antibody with another fluorophore.

Guinea-pig anti Myt1L and rat anti-St18 were raised against the amino acids 267-493 and 60-297 of each protein, respectively. Recombinant proteins were produced (as GST-fusion proteins) and purified and sent to Strategic Bio-Solutions (Newark, De) for antibody production in guinea pig and rat, respectively. Final bleeds were obtained 45 days after immunization.

For imaging, laser scanning microscopy (LSM) and structured illumination microscopy (SIM) were used. When expression levels of a protein between samples were compared, slides/cells were processed side-by-side, and images were captured utilizing identical optical/electronic settings. For protein level quantification in nuclei, LSM images taken under identical parameters were selected for Image J-based particle quantification.

Transmission electron microscopy (TEM) followed established procedure (Zhao et al., 2010). Briefly, handpicked islets were fixed in 2.5% glutaraldehyde in 0.1M cacodylate buffer (pH 7.4) overnight at room temperature. Islets were then washed and treated in 1% osmium tetroxide in 0.1M cacodylate buffer for 1 hour. Islets were then washed, embedded, thin-sectioned for imaging.

Proximity Ligation Assays (PLA), Co-Immunoprecipitation, and Western Blotting

For PLA, islets from adult control and *Syt4*$^{-/-}$mice were isolated and dissociated into small clusters with trypsin (~5-20 cells/cluster). Cytospin were used to attach cells onto slides, followed by fixation with 4% paraformaldehyde for 15 minutes at room temperature. PLA strictly followed manufacturer's instruction. For immunoprecipitation, HEK293T cells were co-transfected with plasmids expressing the cytoplasmic C2 domains of Syt4 (tagged by HA) and Syt7. 48 hours after transfection, cells were lysed by co-IP Buffer (150 mM NaCl, 8 mM Na_2HPO_4, 2 mM NaH_2PO4, 1% NP-40, 0.5% sodium deoxycholate, protease inhibitor cocktails). Cell lysates were mixed with anti-HA magnetic beads (at 4°C for 4 h. The beads were washed with TBST (20 mM Tris-HCl pH7.6, 150 mM NaCl, 0.1% Tween-20) five times, and bound proteins were analyzed by Western blotting.

Free Cytoplasmic Ca^{2+} Recording

Ca^{2+} recording and analysis followed published methods (Jacobson et al., 2010). Briefly, islets were cultured on ploy-lysine coated glass for 48 hours in RPMI medium containing 10% FBS and 11 mM glucose. Islets were loaded with 2 mM FURA2AM (Invitrogen) for 25 minutes in culture medium followed by 20 min starvation in REC buffer (119 mM NaCl, 2.5 mM $CaCl_2$, 4.7 mM KCl, 10 mM Hepes, 1.2 mM $MgSO_4$ and 1.2 mM KH_2PO_4) with 2mM glucose. Islets were then transferred to REC buffer with 2.8 mM glucose for three minutes for recording before stimulation. Buffer changes were achieved by perfusion at 2 ml/min. Stimulating glucose and KCl were 20 and 25 mM, respectively. Imaging was performed using a Nikon Eclipse TE2000-U microscope. The ratios of emitted fluorescence intensities at excitation wavelengths of 340 and 380 nm (F340/F380) were determined every 5 second. The total Ca^{2+} was calculated using a fura-2 calibration kit (Grynkiewicz et al., 1985).

Gene Expression and GSIS Assays in Human EndoC-βH1 Cells

Human EndoC-βH1 cells were grown in DMEM containing 5.6 mM glucose, 2% BSA, 50 μM 2-mercaptoethanol, 10 mM nicotinamide, 5.5 μg/mL transferrin, 6.7 ng/mL selenite, 100 units/mL penicillin, and 100 units/mL streptomycin (Ravassard et al., 2011). For gene overexpression, cells were infected with lentiviral particles (carrying a human *SYT4* full coding region and eGFP reporter) one day after plating. For siRNA transfection (with a mix of three individual siRNAs), dissociated cells were incubated with siRNA (at 100 nana-molar concentration, with RNAiMax) for 5 minutes before plating. Gene expression assays were performed three days after infection or transfection. For GSIS, cells were incubated with 1mM glucose overnight, briefly washed three times using KRB with 2.8 mM glucose, before insulin secretion assays as described above. The cells were equilibrated in KRB with 2.8 mM glucose for 1 hour before GSIS assays.

QUANTIFICATION AND STATISTICAL ANALYSIS

All experiments contained at least two biological replicas and two technical replicas. For quantifications of β cell mass and replication index throughout the pancreas, the frozen pancreatic block was sectioned at 20 μm intervals. One third of all sections were labeled and scanned using Aperio Scanscope. β-cell mass was then calculated based on the total pancreas weight and the percentage of tissues area that labeled for insulin. For vesicle quantification, images from different sections were used. 30-50 images from different β cells were counted, under double-blind settings (image capture and vesicle counting were done by different personnel).

Statistical analyses utilized standard student T test for pairwise comparisons or One-way ANOVA for comparing multiple groups of data points. A P-value of 0.05 or lower was considered significant. Quantification data were presented as (mean ± SEM). For all assays the "n" noted in all figures and manuscript referred to the number of independent experiments, including both biological replicas and technical replicas.

DATA AND SOFTWARE AVAILABILITY

The accession numbers for β-cell RNA-seq reported in this paper are E-MTAB-2266 (https://www.ebi.ac.uk/arrayexpress/experiments/E-MTAB-2266/) and E-MTAB-6615 (https://www.ebi.ac.uk/arrayexpress/experiments/E-MTAB-6615/).